ABSTRACT

SUN, NING. Lattice Boltzmann Modeling of Heat Transfer in Nonwoven Composite Structures. (Under the direction of Dr. Hechmi Hamouda).

The purpose of this work is to provide an improved evaluation of the thermal properties of nonwoven composites based on numerical simulation of heat transfer through porous media. A review of relevant applications of thermal insulations and related information will help comprehend the mechanism of the thermal conduction in nonwoven composites. Important existing models based on conventional with inherent drawbacks of neglecting some aspects of the structural details algorithms are reviewed and discussed.

Thermal Lattice Boltzmann Method is an inclusive numerical method for solving heat transfer through composites with complex structures and geometries, especially fibrous media with large amount of tortuous voids among fibers. Realistic boundary thermal conditions can also be simply imposed with relatively low computational loads. Additionally, the model is not only valid for simulating porous media with solid phase dispersed in air, but it is also effectively workable on solid-solid systems. Thus, the method is selected and a thermal Lattice Boltzmann Model is developed for such media. To validate the model, resulting temperature profiles and estimated effective thermal conductivities are compared with theoretical solutions and available experimental data of metallic composites. A good agreement is obtain. Subsequently, the relationship between the volume fraction of the reinforcement and the effective thermal conductivity is analyzed and established for various nonwoven composites.

Lattice Boltzmann Modeling of Heat Transfer in Nonwoven Composite Structures

by
Ning Sun

A thesis submitted to the Graduate Faculty of
North Carolina State University
in partial fulfillment of the
requirements for the degree of
Master of Science

Textile Engineering

Raleigh, North Carolina

2011

APPROVED BY:

_____	_____
Dr. Hechmi Hamouda Committee Chair	Dr. Behnam Pourdeyhimi
_____	_____
Dr. Xiangwu Zhang	Dr. Yichao Wu

DEDICATION

This thesis is dedicated to my parents and my little sister for their unconditional love, support and encouragement.

BIOGRAPHY

Ning Sun comes from China. He completed his Bachelor of Textile Engineering in 2005 in Donghua University, China. After completing the undergraduate study, he was employed by Groz-Beckert KG, a German company developing and producing textile machinery components, and working in the Shanghai branch as a sales engineer in felting division. He started with his Master of Science degree in Textile Engineering at North Carolina State University in fall, 2009. He plans to continue his education by pursuing his Ph.D. degree in Fiber and Polymer Science program at North Carolina State University after graduation.

ACKNOWLEDGMENTS

There are many individuals that I want to express my gratitude to. This study would not have been possible without their unconditional support and encouragement.

First of all, I am very grateful to Dr. Hechmi Hamouda who guided me through the two year Master's study. He gave me enough space to study the subjects that I was interested in, and was always supportive for me to have different attempts. Once I have got troubles in study, he was very patient to give me valuable guidance. He is a professor who not only cared about my research, but also offered me a lot of advices and help for my life in the US. When I decided to continue for my PhD degree, he completely supported my plan and took his own experience as an example. I sincerely appreciate his understanding, support and tolerance to me in the two years. I am also very grateful to Dr. Behnam Pourdeyhimi, Dr. Eunkyoung Shim, Dr. Jon Rust, Dr. Xiangwu Zhang and Dr. Yichao Wu, who played pivotal role during my study. I would like to thank Ms. Angie Brantley for making sure all my forms in order and being patient to answer every question that I had.

I would like specially to thank my best friend, Jun Zhang, a PhD student in Civil Engineering at North Carolina State University. Setting up a numerical model was a completely new topic for me before this study. Jun has spent hour by hour sitting with me to explain the relevant concepts and procedures. We had many intense arguments when there were different understandings; whereas our friendship was strengthened at the same time. Thank you so much, Jun, for your concern, patience and kind help.

TABLE OF CONTENTS

LIST OF TABLES

LIST OF FIGURES

1. Introduction

1.1. Nonwoven Composites

Nonwovens are fabrics manufactured directly from fibers by mechanical, chemical or any other possible means or the combination of technologies to entangle fibers together, so that unique fabric structures are obtained. Fibers are randomly distributed in the structure and significant amount of voids are obtained between fibers. The size of voids and the volume fraction are determined by the specific web forming and boding techniques as well as the production configurations. Nonwovens are not only closely connected to people's daily life, but also widely applied in many other fields, such as automotive, aerospace, construction etc. Specific nonwoven thermal properties can be designed based on each application requirements.

Filtration, thermal insulation and noise absorption are among the important application characteristics if not the most dominant ones. Although these applications seem different, there are a lot of similarities among these phenomena especially when their associated diffusion processes are considered. Heat flow (mostly infrared waves) and sound waves are capable of propagating through both the fiber component and the air component, whereas dirt particles diffuse through voids. The solid-fluid interfaces provide the main effect of the dissipation on energies and the amount of particles. Therefore, no matter what medium transmitting through the nonwoven composites, the amount of voids is the determining factor for all final results.

Nonwoven is a perfect filter capable to capture and trap very fine particles within the tortuous voids along the paths of contaminated fluids flowing through the media. Producing microfiber web and charging fibers with electrostatic during fiber spinning are both popular filtration enhancement techniques in this application. Microfibers increase the contact surface area with particles and reduced the size of pores; and electrostatically charged fibers attract fine contaminants attached on the surface, thus making the filtration more efficient through control of the diffusion and transport processes.

Nonwoven media also have superior performances in noise absorption applications in buildings and automotive applications. When sound waves propagate through a fibrous network of interconnected void spaces, diffusion dumping and thermal effects cause acoustic energy to be dissipated and absorbed. Fiberglass and petro-based fibers are leading materials though; broad variety of materials can be applied for sound absorbing structures such as ceiling tiles, carpets and headliners in vehicles. [1, 2]

Nonwoven composites as thermal insulators are another important product widely applied in buildings, vehicles, microwave ovens etc. Fibers with good mechanical properties but poor thermal insulation performance are embedded in matrices (air for nonwovens) which have better thermal resistance. In this manner, the overall mechanical and thermal insulation properties of these composites are improved compared with their individual components. It is commonly known that nonwovens with fibers encapsulating in air voids have effective thermal conductivities significantly lower than those of pure fibers, because air is an excellent insulator with great thermal resistance represented with the R-value ($R = 5.5/inch$) as long as convection is restrained.

A significant amount of heat is produced from internal combustion engines and green-house effect during their transport vehicle usage. Thus, thermal insulators are installed around the engine compartment and throughout the vehicle to prevent direct exposure of passengers and heat-sensitive components to heat. This insulation is also needed to isolate passengers from the element during summer and winter extreme weathers. PET (Polyethylene Terephthalate) nonwoven felts are commonly applied in vehicles for thermal insulation due to their high mechanical and thermal properties. The felts are sometime coated with thin metallic foil for high temperature environments [3].

This trend of thermal isolation usage is increasing since according to the statistics conducted by the International Organization of Motor Vehicle Manufacturers (OICA), car production and sales reached maximum value in 2007 with 55 million units. Although a slight decline was apparent as a result of the economy recession afterwards with 53 million units in 2008 and 52 million units in 2009, there was still an impressive growth compared with the sales volume during last decade [4]. About 20 kg of textile products are used in every car and about 11% of these are nonwoven composites, mostly applied as headliners, floor carpets, insulations etc.. Nonwovens are selected for many applications because they are cost efficient, moldable and due to their high thermal insulation as compared with conventional textile fabrics [5].

Similarly construction is another area adopting large amount of fibrous insulators to control the internal dwelling climate and to maintain occupants comfort. Saving energy and making efficient use of energy so as to reduce unwanted heat loss or gain are also essential reasons of applying additional insulators. According to statistics conducted in the UK, 50MWh of

electricity is consumed annually by an average dwelling resulting in 12,000 GJ of energy over a 50-year period: the average lifespan of a US dwelling. More than 60% of the energy is spent on space heating and cooling for households as shown in Figure 1.1. An improved thermal insulation envelope is one of the best ways to prevent energy loss. [6]

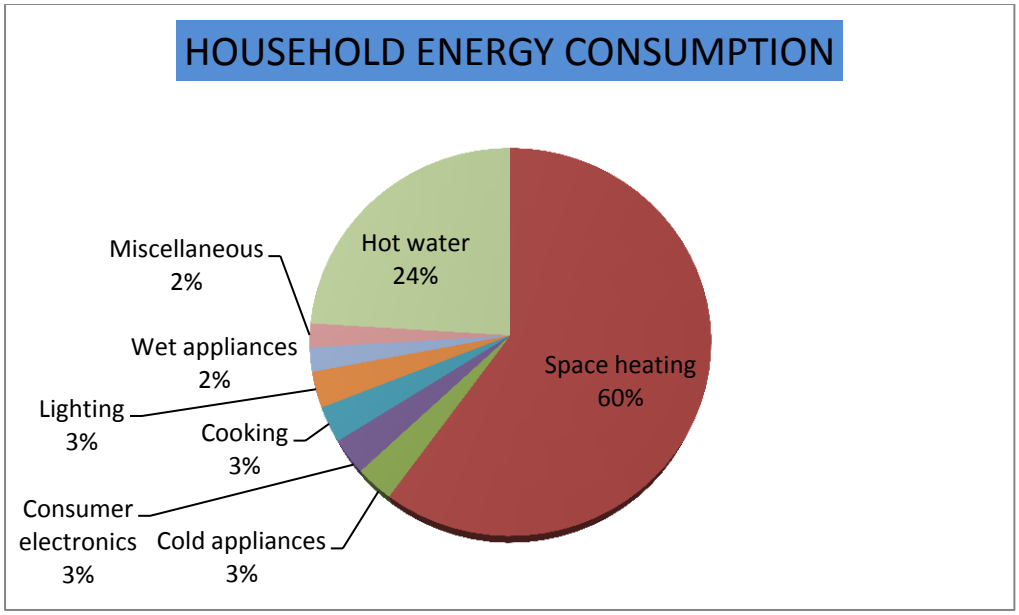

Figure 1.1: Percentages of Household Energy Consumed on Different Areas [DTI 2004].

A wide variety of materials is utilized for thermal insulation, such as cellulose, glass wool, rock wool, polystyrene etc. House builders are not only developing high-efficient thermal insulators but also trying to improve the thermal insulation performance of other building components such as concrete blocks. Another attempt with great popularity is the addition of scrap-tires to concrete for construction, especially in Portland cement concrete. Subsequently, the obvious enhancement of concrete thermal insulation performance has been observed and reported. [7, 8] Bulent Yesilata et al. proposed to add PET (Polyethylene Terephthalate) waste pieces from recycled bottles to concretes for the same purpose. The

resulting composite was tested using an adiabatic hot-box technique, and a significant improvement of 18.16% was achieved compared to ordinary concrete. Similar percentage increase was also shown for concrete with added rubber chunks. [9]

1.2. Bio-nonwoven Composites

Bio-materials draw a great deal of researcher's attention as substitutes of petro-based polymers because of the increasing concerns about environmental protection, efficiency of energy consumption and control of production cost. Bio-nonwoven composites are broadly considered as nonwovens manufactured from a wide variety of agro-based fibers i.e. cellulosic fibers or animal i.e. protein fibers or mineral fibers as reinforcement components. Biodegradable resins for better mechanical and thermal compliance are also considered as matrices for these composites. [10 - 12]

Bio-nonwoven composites are most of the time bio-degradable, recyclable and obtained from a renewable source. Agro-based/cellulosic fibers are the most popular raw materials produced as agricultural crops, such as hemp, jute, flax etc. Thus, less energy and capital investment is required for production. As an initial experiment, a group of fiber was assessed as an introductory work for the thesis. There fibers have superior physical properties, as shown in Table 1.1, compared to petrol-based fibers, especially in terms of their specific tensile properties (known value normalized by material density). The gain in properties is due to the relatively low densities of these materials [13, 14].

Table 1.1: Physical Property of Bio-fibers and Synthetic Fibers [12-14].

Fiber	Density ($g/cm^{3)}$	Tensile Strength (MPa)	Young's Modulus (GPa)	Elongation at Break (100%)
Cotton	1.5-1.6	287-800	5.5-12.6	7.0-8.0
Jute	1.3-1.45	393-773	13-26.5	1.16-1.5
Flax	1.5	345-1100	27.6	2.7-3.2
Hemp	—	690	—	1.6
Ramie	1.5	400-938	61.4-128	1.2-3.8
Sisal	1.45	468-640	9.4-22.0	40609
PALF	—	413-1627	34.5-82.51	1.6
Coir	1.15	131-175	40639	15-40
E-glass	2.5	2000-3500	70	2.5
S-glass	2.5	4570	86	2.8
Aramid	1.4	3000-3150	63-67	3.3-3.7
Carbon	1.7	4000	230-240	1.4-1.8

However, one of the major drawbacks of using natural fibers is associated with their significant property variations. This is resulting from the diversity of available resources with different harvest conditions and growth locations. Therefore, it is of importance to identify the properties of individual fibers and seek out a blending configuration with optimized properties. Kenaf, flax, jute, hemp, kapok and cotton fibers were made for evaluation. Then

the morphologies of these cellulosic fibers are assessed using a Nikon Eclipse 50i Polarizing Optical Microscope. The results are shown in Figure 1.2.

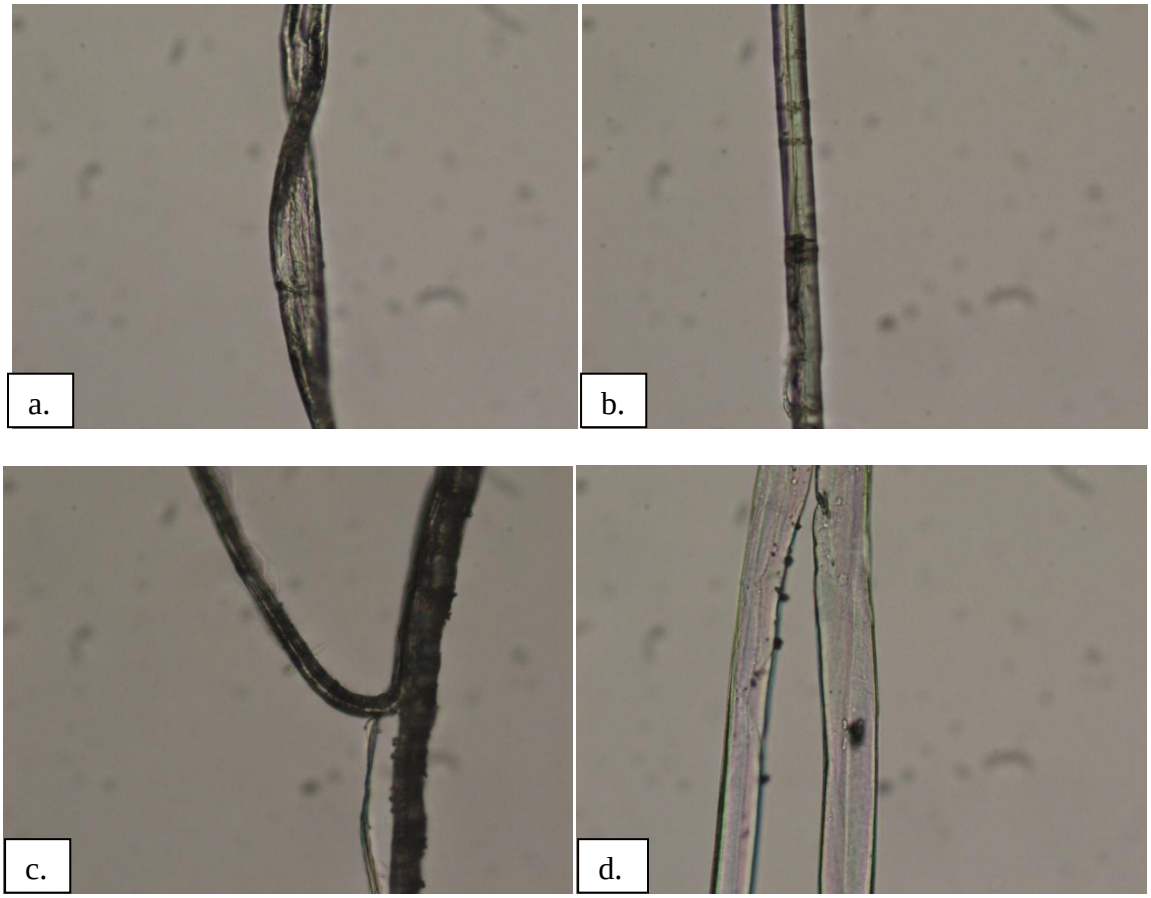

Figure 1.2: Different Fibers' Morphology Images (Magnification: x50): a. Cotton; b. Flax; c. Hemp; d. Kapok.

The fiber diameters of each variety are measured and presented in Table 1.2 with their calculated fiber fineness.

Table 1.2: Fiber Diameters of Available Fibers.

	Diameter (μm)					
Sample #	**Flax_a**	**Flax_b**	**Jute**	**Hemp**	**Kapok**	**Cotton**
1	9.7	3.5	27.0	11.0	12.0	8.0
2	7.0	9.0	27.3	7.0	8.1	5.0
3	7.5	9.0	29.7	4.8	7.0	6.0
4	6.0	4.0	19.7	9.9	7.0	11.0
5	8.0	3.9	21.0	9.8	9.2	6.5
6	2.2	41.0	26.0	6.8	8.0	12.0
7	8.0	6.9	32.4	11.5	10.0	6.7
8	3.6	6.0	26.8	4.2	6.1	7.0
9	4.5	9.0	25.1	11.0	12.0	7.2
10	6.2	8.0	29.0	11.7	9.0	8.0
Mean	6.3	6.6	26.4	8.8	7.7	8.8
Fineness (Denier)	1.9	2.1	27.1	3.4	0.7	3.0

V.G. Yachmenev et al. have shown that cellulosic-based nonwoven composites have excellent thermal insulation properties. Different fiber compositions were designed and their insulations were measured with a Steady-State Heat Flow Meter. Lower thermal conductivities and thermal transmittance of composites were observed with the amount of cellulosic fibers replacing polymeric fibers in composites. However, the thermal insulation properties of the bio-nonwoven composites varied significantly depending on the type of cellulosic fibers, the ratio and the nature of the binder and the structural properties of the composites. [5, 15]

Moreover, the European Union automotive legislation, once established by the end of 1999, requires that 85% of disposed vehicles (by weight) should be reusable and recyclable by 2005 and this rate is expected to increase up to 95% by 2015 [5, 13, 14]. Since most petro-based polymers take long time to degrade under ambient conditions, it is a valuable start to replace part of synthetic fiber with bio-materials, thus, enhancing bio-degradability. Meanwhile, such approach will maintain and also improve the thermal and acoustic insulation requirements since bio-fibers inherently have higher thermal insulation characteristics. Thus, bio-composites have a promising future with market share growing in automotive and other industrials applications.

Therefore, it is of significant importance to accurately determine the thermal and other associated characteristics of nonwoven composites, in order to develop improved and optimized products for such applications.

Two approaches are actually available nowadays for investigating thermal properties of materials based on their experimental measurements or numerical simulations. Both of these

approaches have advantages and drawbacks. The experimental approach requires that a large amount of samples has to be manufactured and exposed to overcome material and manufacturing variations; meanwhile, repeated exposures and measurements have to be conducted to reach a reasonable assessment results. However, experimental results are easily understandable and accurately reflecting the real characteristics of the materials.

For numerical models, an understanding of the relevant fundamental theories is required as well as the details of the materials microstructure. An approximation is calculated from the model, while the computational time would increase if higher accuracy is pursued; whereas this model is capable to predict properties of materials with similar structures once the model is developed. Then repeated experimental testing become less necessary; energy and time are significantly saved as a result.

This study is to develop a numerical method for predicting the effective thermal conductivity of nonwovens and other composites with complex two-phase porous structures. It is of importance to review the heat transfer mechanisms within a fibrous structure before developing the model.

1.3. Heat Transfer Mechanisms

Heat transfer is a common phenomenon that is closely associated with every aspect of life; however, in spite of its associated complex processes, it can be reduced to its basic characteristics: It mainly concerns the exchange of thermal energy from one physical system to another in three basic mechanisms including heat conduction, convection and radiation. A temperature gradient is the only drive of heat transfer, because a thermal potential is formed between the warm and cool region, so that heat flows from the former to the latter.

An inclusive heat transfer model based on combining all three mechanisms is introduced here to describe how thermal energy is transported in nonwoven composites. And the following is an explanation of the assumptions that are applied for formulating the model as well as the program listings for the heat transfer numerical model.

To represent, in a simple manner, the heat transfer process through a nonwoven structure for insulation applications, it is important to assume that the temperature is constant and evenly distributed all over each single plane perpendicular to the heat flow direction, and that all local three modes of heat transfer are independent. Additionally, radiation, gas conduction and solid conduction are summed to be the sole heat flux through these planes [16]. Gas conduction terminology is consisting of the heat transferred in conduction and convection through a gas phase. The former is taking a very small proportion compared with the latter because of the low thermal conduction of air compared to its high convective property. The overall heat flux, q, can be considered to be:

$$q = q_r + q_g + q_s \tag{1}$$

Where:

q_r*: Radiation heat flux*

q_g*: Gas conduction heat flux*

q_s*: Solid conduction heat flux*

The overall heat flux or the rate of heat conduction through a nonwoven composite is proportional to the temperature difference, ΔT, across the material and inversely proportional to the distance, L, between the two temperature levels, i.e. [16]

$$q = K\frac{\Delta T}{L} \quad (2)$$

Therefore, the overall effective thermal conductivity, K_{eff}, could be expressed by superposition of the solid conduction, K_s, gas conduction, K_g, and radiation, K_r, within the expression of the heat flux as the following configuration:

$$K_{eff} = K_s + K_g + K_r \quad (3)$$

However, these terminologies are different from the real conductivities of solid and gas components, and are determined by the proportion of each component and their corresponding distributions etc.

1.3.1. Convection

Convection is due to the motion of gas or fluids transporting heat, which is caused by a temperature gradient. Generally, when a fluid is heated, it becomes buoyant and flows towards the denser or cool side. To compensate, in an enclosure, an opposite movement appears for the sinking denser fluid, so that a convective flow circulation or current is formed. If allowed out of the enclosure, this is the major mean the energy loss via air flowing or leaking in and out of buildings.

Since the air contained within a fibrous structure is trapped in tortuous voids without any overall air circulation between the structure and its surrounding, convection effects are neglected in this numerical model. The heat energy circulating through convection remains trapped within the structure. Additionally, nonwoven insulations investigated here are always

contained between two solid facings, which prevent air transport in and out of the insulation composites.

1.3.2. Radiation

Radiation is the transfer of electromagnetic wave, mainly Infrared waves, through a transparent medium. When exposure between two bodies with different temperature occurs, radiation occurs and a subsequent rise in the temperature of the cold body. The sun light warming up the earth is good example illustrating radiation.

Radiant heat transfer with in fibrous structures plays an important part, during heat transfer, in most circumstances, even in cryogenic insulation [16]. Radiation can be described as the sum of scattering, absorbing and emitting heat when transmission through voids takes place. Radiation is weakened when traveling along a tortuous path because of absorption and scattering, whereas enhanced by emission. Absorption occurs in transmission of electromagnetic waves mainly infrared radiation (Wavelength between: 1μm and 50μm). Scattering occurs at interfaces between air and fibers with a discontinuity in refractive index. The extinction coefficient, E, [17] is the sum of absorption coefficient and scattering coefficient (Table 1.3 and Table 1.4). Both of these coefficients depend on operational medium temperature, pressure and wavelength [16].

Table 1.3: Mean Specific Extinction Coefficients for Fiber Layers and Opacifiers in the Wavelength Region between 1 μm to 50 μm at $T_r = 300\ K$ [17].

Material	Particle or Fiber Φ /(μm)	e /(m^2kg^{-1})
5% Fe_3O_4 in fumed silica	2	40
5% TiO_2 in fumed silica	2.5	40
Soot	<0.1	600
Glass Fiber	5	50
SiO_2 Fiber	10	30
Al_2O_3 Fiber	4	50

The extinction coefficient is of great importance since it represents the energy decay during transmission. The coefficient is the reciprocal of the radiation mean penetration distance and is expressed, in m^{-1}, as: [16-18]

$$E = e * \rho \tag{4}$$

Where:

e: Specific extinction coefficient of the fiber medium

ρ: Density of the fibrous layers

Thus, the radiative conductivity can be expressed as:

$$k_r = \frac{16\sigma n^2 {T_r}^3}{3E} \tag{5}$$

Where:

σ: Stefen-Boltzmann constant

The mean index of refraction, n, of the porous layer can be calculated with the following equation:

$$n = 1 + (n_0 - 1)\frac{\rho}{\rho_f} \tag{6}$$

Where:

n_0: *The index of refraction of the porous layer*

ρ_f *: Fiber density*

The mean radiative temperature, T_r, has different understandings. And here the definition advanced by J. Fricke et al. is applied as the following relationship between the temperatures of the hot, T_1, and cold, T_2, boundaries: [17]

$$T_r^3 = \frac{(T_1 + T_2)(T_1^2 + T_2^2)}{4} \tag{7}$$

The following study is used as an illustration to show that at ambient temperature the radiation effects can be neglected: Anastasios Karamanos et al. have calculated the thermal conductivity of stone wool at different temperature from 25°C to 1000°C. Their results indicated that the solid and gas conductivity were about ten times greater than radiative conductivity when temperature is below 100°C; and then the radiative component rises sharply after that temperature level. The results are shown in the Table 1.5 and plotted in the Figure 1.3. [19] M. Spinnler et al. have made similar results showing that the proportion of radiative effects is relatively small compared with the effects of thermal conduction at

ambient temperature condition in the overall heat transfer mechanisms. However, the radiative effects do become significant when the temperature is greater than 300°C (Figure 1.4) [20]. Based on these studies, it is therefore acceptable to neglect the effects of radiation when ambient temperature conditions are applied.

Table 1.4: Absorption and Scattering Coefficients for Several Insulating Materials [16].

Material	**Density (kg/m^3)**	**Diameter (m)**	**Temperature (K)**	**Absorbing (m^{-1})**	**Scattering (m^{-1})**
Borosilicate glass fibers	200	$1*10^{-6}$	500	1,300	26,000
			600	1,100	27,000
			800	1,100	28,000
			1,000	700	3,100
			1,700	600	2,500
Silica fibers	50	$1*10^{-5}$	500	200*	3,300
			650	200*	5,000
			800	100*	710
			1,000	100*	740
Carbon fibers	65	$1*10^{-5}$	775	400	38,500
			923	200	26,000
			1,123	200	18,500
			1,273	400	20,000
Polyurethane foam	35	Random pore size	500	200	2,850

* These listed values are upper limits.

Table 1.5: Model Results for Calculated Conductivities [19].

	Thermal Conductivity (W/m*K)			
Temperature (^{o}C)	K_r	K_g	K_s	K_{eff}
25	0.0011	0.0262	0.0224	0.0269
50	0.0014	0.0276	0.0220	0.0284
75	0.0017	0.0290	0.0216	0.0300
100	0.0021	0.0304	0.0213	0.0316
250	0.0058	0.0389	0.0200	0.0426
500	0.0186	0.0530	0.0194	0.0677
1000	0.0832	0.0813	0.0165	0.1561

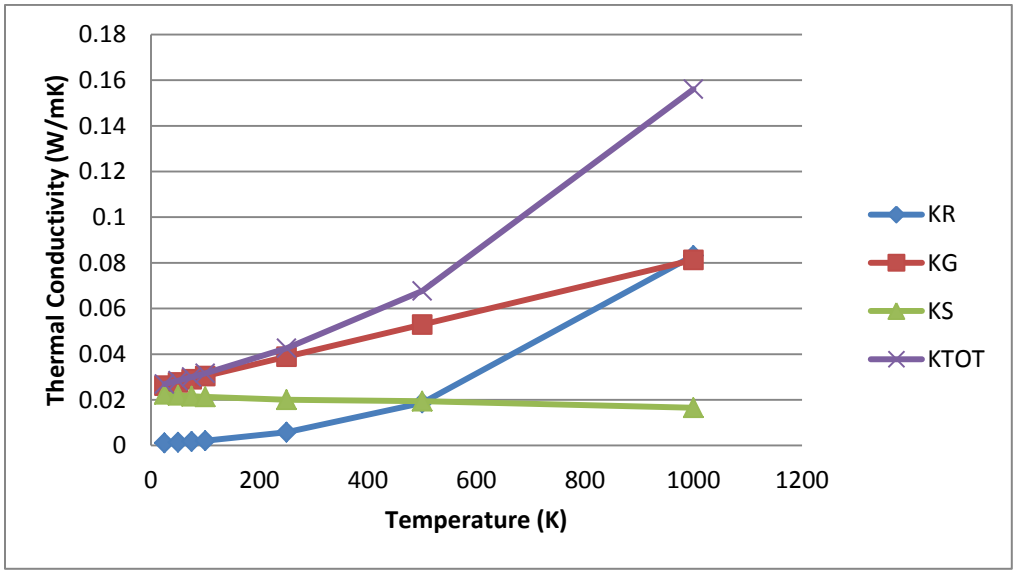

Figure 1.3: Conductivities Calculated with Anastasios's Model for a Wide Temperature Range.

1.3.3. Conduction

Conduction is the heat energy transfer between molecular collisions due to direct contact. The better the conductor, the faster heat will transfer. Most metals are good conductors, whereas wood, Styrofoam, paper and air are insulators with small conductivity values.
A pure thermal conduction is assumed in the numerical model with the effects of convection and radiation neglected. Solid conduction does not significantly change as temperature is rising; whereas gas conduction does show an obvious increase, because collisions among molecules become intense at high temperature and cause faster energy transfer. The phenomenon has been proved by M. Spinnler et al. in their works using the Rosseland approximation to analyze combined heat transfer in multilayer thermal insulations [20]. The results are shown in Figure 1.4.

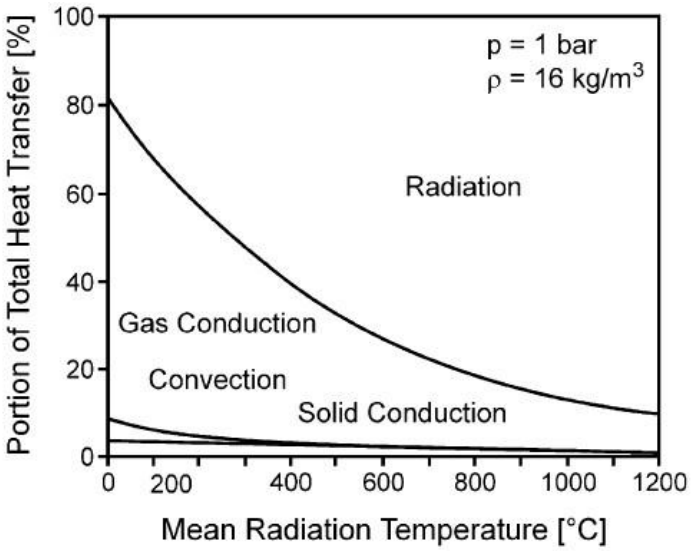

Figure 1.4: Rosseland Portions of Heat Transfer Mechanisms in a Ceramic Fiber Mat of Low Density [20].

Thermal conduction of a fibrous material depends not only on the thermal properties of each component (fiber and air), but also greatly on the structure of the medium with volume fraction of voids (porosity), fiber size, fiber orientation and mass distribution. Some models have been developed for simulating the thermal conductivity of fibrous media as an additive term of the properties of individual phase. However, these models did not consider the system as an integral structure and overlooked the interaction between components. Realistic boundary conditions were not precisely applied to ensure the proper accuracy for each model.

1.3.3.1. Solid Thermal Conductivity

J. Fricke et al. 's model dealing with the solid conduction proportion, K_s, as depending on the real fiber conductivity, K_f, and Young's modulus, Y_0, of the fiber material and porosity, Π, of the layer and pressure imposed upon the layer, P_{ext}, as well as fiber orientation etc [17, 20].

$$K_s = K_f f(\text{п}, Y_0, P_{ext}) \tag{8}$$

$$f = \frac{16}{\pi^2}\left[\frac{Y_0^{\frac{1}{3}}}{(3 * \pi^2(1-\mu^2)(1-\text{п})^4 P_{ext})^{1/3}} + \frac{1}{4(1-\text{п})^3}\right]^{-1} \tag{9}$$

Where:

μ: *Posson's ratio of the fiber material,* $\mu^2 \ll 1$

Y_0: *Young's modulus, required to be large* $\approx 10^{10} N/m^2$

The above function is applicable based on the Kaganer's Lattice model. The model assumed that the number of contacts between fibers and the porosity remain unchanged upon compression, when crossing fibers are arranged regularly in plane normal to the heat flow.

However, in practice, both of the parameters have to be changed upon compression. Thus, the function was modified to account for the change on porosity:

$$\pi = 1 - \frac{\rho}{\rho_f} = 1 - \frac{m''}{d} \tag{10}$$

Where π is about 90% for fleece-type fibrous insulations, and

m'': *Insulation fiber mass per unit area*

d: *Thickness*

Another model for solid conductivity was introduced by Anastasios K. et al. in their works [19]. The thermal conductivity for solid phase is expressed as follow:

$$K_s = f_\rho^2 * K_f \tag{11}$$

Where:

f_ρ: *The ratio of insulation material density to the fiber's materials density*

A similar model for the thermal conductivity of the solid phase was developed by Markus S. et al and where the conductivity, as function of processing temperature, is evaluated as: [20]

$$K(T)_s = {f_v}^3 * K_f(T) \tag{12}$$

f_v: *Fiber volume fraction*

These models have been validated in their respective studies. However, the accuracy would be questionable, because the details of fibrous structures were not considered: by controlling the fiber fraction, fiber orientation distribution, fiber connections and surface areas are all capable to significantly vary the resulting thermal conductivities of the fibrous component.

1.3.3.2. Gas Thermal Conductivity

Anastosios K and Kamran D. both characterized the thermal conductivity for the gas phase with the Knudsen number, Kn, in their respect works. [16, 19, 21, 22] The Knudsen number is a dimensionless number defined as the ratio of the molecular mean free path length, λ, to a representative physical length scale, and can be expressed as:

$$Kn = \frac{\lambda}{Lc} \tag{13}$$

Where:

This length scale, *Lc*, is also called the characteristic length, and can be obtained with the following equation:

$$Lc = \frac{\pi D_f}{4 f_\rho} \tag{14}$$

Where:

D_f *: Fiber mean diameter*

The middle free path of air's molecules is also called as the ideal-gas mean free path. For the atmospheric air, λ is about $6 * 10^{-6}$cm or 0.06μm. λ is determined with the following relationships:

$$\lambda = \frac{K_B T}{\sqrt{2}\pi d_g^2 P_{ext}} = \frac{16V}{5\rho_g\sqrt{2\pi RT}} \tag{15}$$

Where:

K_B: *Boltzmann constant, 1.3806*10^{-23} [J/K]*

d_g: *Air's collision diameter [m]*

V: *Dynamic Viscosity [pa*s= (N*s)/m^2]*

ρ_g: *Density of air [g/cm^{-3}]*

R: *Gas constant*

T: *Absolute temperature [K]*

After defining the Knudsen number, the effective thermal conductivity of the gas, K_g, component can be calculated:

$$K_g = \frac{K_g^*}{\emptyset + 2 * \Psi * \frac{2-\alpha}{\alpha} * \frac{2*\gamma}{\gamma+1} * \frac{1}{Pr} * Kn} \qquad (16)$$

Where:

K_g^*: *Thermal conductivity of the gas* $[W.m^{-1}.K^{-1}]$

Pr: *The Prandtl Number*

The Prandtl Number, the ratio of momentum diffusivity (viscous diffusion rate) to thermal diffusivity. For air and many other gases Pr is in the range of 0.7-0.8; and can be calculated with the following relationship [16].

$$Pr = \frac{v}{\alpha} = \frac{viscous\ diffusion\ rate}{thermal\ diffusion\ rate} = \frac{C_p V}{K_g^*} \qquad (17)$$

Where:

$v = \frac{V}{\rho_g}$ *: Kinematic viscosity [m^2/s]*

C_p: *Specific heat [J/ (kg*K)]*

The thermal accommodation coefficient, a, is the factor representing the energy exchanged between surrounding air a_1 and fiber's materials a_2. This coefficient is equal or less than 1 and can be evaluated based on the following relationship:

$$a = \frac{a_1 a_2}{a_2 + a_1(1 - a_2)} \leq 1 \qquad (18)$$

Where:

a_1 , a_2: *The two surface accommodation coefficients*

γ: *Specific heat ratio of air*

Φ, Ψ are parameters which specific values depend on the value of the Knudsen number:

Φ = 1, Ψ=0, when Kn < 0.01,

Φ = 1, Ψ=1, when 0.01 < Kn < 10

Φ = 0, Ψ=1, when Kn > 10

Gas conduction is one of the major mechanisms of heat transfer through the air in voids of nonwovens. Across the range of important applications, it may involve both continuum and non-continuum conductions. A continuum condition is defined at $Kn \leq 0.01$ (continuum regime) with gas conduction characteristic length significantly greater than the molecular mean free path. There is significant amount of air molecular collisions occurred and caused a high thermal condition. On the contrary, when $Kn > 10$ (free-molecular regime), the molecular density is extremely low and very few collisions between gas molecules occurred; then heat transfer in conduction is little. Air molecules move back and forth only when colliding with the two solid boundaries. Between these two extreme conditions, when $0.01 <$

$Kn < 10$, both kinds of collisions exist; and the status is called the transition and the slip or jump regimes [16, 19, 21, 22].

1.3.3.3. Effective Thermal Conductivity

When solid conductivity and gas conductivity are evaluated, it is necessary to consider how to combine the thermal conduction effect of each phase together. The sum of the individual conductivities according to their corresponding volume fractions is the simplest approach to approximate the effective thermal conductivity, K_{eff}.

$$K_{eff} = f_v K_s + (1 - f_v) K_g \tag{19}$$

However, the results estimated with this simple model are far from the realistic ones. Thus, Anastasios K. et al have proposed a method to integrate the thermal conductivities of gas and solid phases. In this method, not only the volume fraction of each component or phase are considered, the fiber orientation distribution is also involved and roughly categorized into three groups according to the fiber orientation to the heat flux direction. The effective thermal conductivity can then be calculated: [19].

$$K_{eff} = K_s + \frac{K_g - K_s}{1 + \frac{f_v}{1 + f_v}[1 + z * \frac{K_g - K_s}{K_g + K_s}]} \tag{20}$$

Where:

z: *Coefficient of fiber orientation distribution takes the values:*

$z = 1$, *when fibers are oriented vertical to the heat flux direction*

$z = 2/3$, *when fibers are randomly oriented*

$z = 5/6$, *when the 50% of fibers are oriented vertical to the heat flux direction and the other 50% are randomly oriented*

1.4. R-value

R-value is a measure of thermal resistance for insulations. As previously expressed, heat flux is the product of conductivity and temperature gradient. Then U-value is introduced to characterize the ability of the medium to conduct heat from one side to the other, e.g.

$$q = U(T_{in} - T_{out}) \tag{21}$$

For the insulation batts that are applied in construction as shown in Figure 1.5, the U-value, expressed in $BTU/(ft^2 \cdot h \cdot °F)$ or $W/(m^2 \cdot °C)$, can be defined as: [23]

$$U = \frac{q}{T_{in} - T_{out}} \tag{22}$$

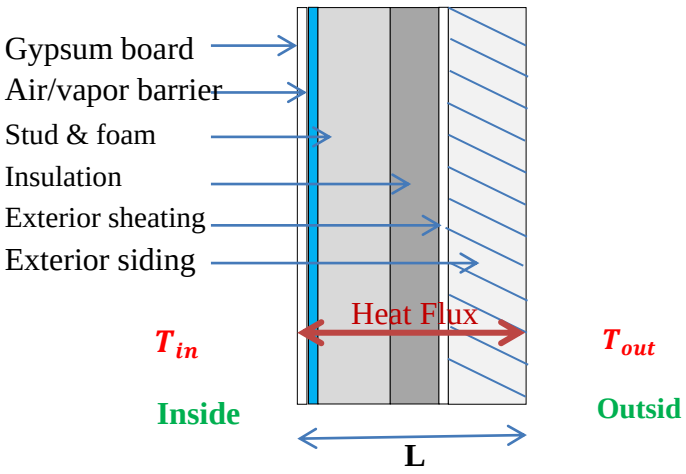

Figure 1.5: Schematic of Components of a Wall.

Therefore, the heat flux, q , is the same throughout each layer, and the value is equal to the U-value of each individual layer multiplied by its temperature gradient:

$$q = U_1(T_0 - T_1) = U_2(T_1 - T_2) = U_3(T_2 - T_3) = U_4(T_3 - T_4) = \cdots \quad (23)$$

Here, the total temperature difference is the sum of the temperature differences of each layer:

$$\Delta T = T_{in} - T_{out} = (T_0 - T_1) + (T_1 - T_2) + (T_2 - T_3) + (T_3 - T_4) + \cdots \quad (24)$$

The overall temperature gradient across the batt can be also expressed as:

$$\Delta T = \frac{q}{U_1} + \frac{q}{U_2} + \frac{q}{U_3} + \frac{q}{U_4} + \cdots \quad (25)$$

Thus, the R-value is defined as the reciprocal of the U-value, and the temperature difference can be presented as:

$$\Delta T = (R_1 + R_2 + R_3 + R_4 + \cdots)q \quad (26)$$

Here, the R-value of a material is used to indicate the Resistance to transfer heat from one side to the other; and it can be expressed in $(ft^2 * hour * °F)/BTU$ or $m^2 * ℃/W$. The higher the R-value of a material, the better thermal insulation it provides. R-value is more practical to describe the thermal characteristic than the U-value, because the former is an additive property when materials are arranged sequentially.

R-values for some common building materials are listed in Table 1.6; and shows that stone, brick and concrete are actually poor insulators. Static air is an excellent insulator.[23]

To have an improved understanding on how the R-value is applied to indicate the thermal resistance property in industry, a traditional wall with the configurations shown in Figure 1.5 is shown as an example. The detailed R-value for each component is represented in Table 1.7 [23].

The R-value is unimportant factor for common building standard. Then it becomes crutial to have an efficient method for obtaining R-values for materials of interest. R-value is mainly determined by the thermal conductivity of each composite, and it is necessary to be assessed for all used products.

Table 1.6: R-values for Some Common Building Materials [23].

Items		**R-value**
1/2-inch sheetrock drywall		0.64
0.50in outsider plywood		0.62
Rough Sawn cedar siding		1.25
Aluminum, steel or vinyl siding (hollow backing)		0.61
Asphalt roof shingles		0.44
Concrete blocks		1.04
Dual-pane windows		1.92
Triple-pane windows with argon gas		5.88
Brick (common size)		0.20/inch
Pine wood		0.95/inch
Concrete		0.09/inch
3-5-in fiberglass batt insulation		13
Biobased Insulation 1701	2.0 inches	12
	3.5 inches	19
	5.0 inches	28
Cellulose spray		3.42/inch
Icynene®-spray		3.6/inch
Icynene®-pour formula		4.0/inch
Urethane foam		5.3/inch
Expanded polyurethane		6.2/inch
Polyiso foam		7.62/inch
Air		5.5/inch

Table 1.7: R-values of each Component in a Traditional Wall [23].

Component	R-value
Still air inside-thermal layer	0.68
Paint	Negligible
½-inch sheetrock	0.64
6-mil plastic-moisture barrier	Negligible
3.5-inch batt insulation	13.00
½-inch exterior plywood	0.62
1-inch foamboard	5.00
Rough sawn cedar shingles	1.25
15 mph wind outside-thermal layer	0.17
Total R-value	21.36

1.5. The Guarded-Hot-Plate Apparatus for Thermal Conductivity

There are various test methods and testing equipments that are relevant to the evaluation of thermal transmission properties. These methods can be categorized into two groups: with the steady-state methods and the transient (dynamic) methods [24]. The former category includes the Guarded-Hop-Plate Apparatus (ASTM C177), the Heat Flow Meter Apparatus (ASTMC518) and Hot Wire Method (ASTM C1113) etc. Once the heat flux is determined based on a temperature profile, the thermal conductivity of specific materials could be derived. The latter, such as the Dynamic Adiabatic-Box technique, the Lasher Flash method

and the TP02 Non-Steady-State Probe (ASTM D5334-92, D 5930-97) are based on the temperature versus time response of the sample when subjected to a constant heat flux [24]. Then the thermal diffusivity and the thermal conductivity can be obtained. The Dynamic Adiabatic-Box technique is proposed by Bulent Yesilata et al. and applied in their work for measuring the insulation properties of concretes combined with PET waste and rubber pieces [9, 24].

The Guarded-Hot-Plate Apparatus is a widely used and versatile method for measurement of steady state thermal transmission. The method is based on a simple operation and provides accurate results for flat, homogeneous materials with low thermal conductivities at a moderate temperature condition [24-26]. The main components of an idealized system with a double-sided mode are illustrated in Figure 1.6. Generally, the apparatus, located in an environmental chamber, consists of a hot surface assembly comprised of a guarded-hot-plate (aka. metered section) and a primary guard, two cold surfaces assemblies, and a temperature-controlled secondary guard. The metered section is defined by ASTM C177 as the portion of the test specimen (or auxiliary insulation) through which the heat input to the guarded-hot-plate flows under ideal guarded conditions [26].

Two identical samples are sandwiched between the hot surface assemblies, which provide the steady-state, one-dimensional heat flux through the specimens. The cold surface assembly is considered as isothermal boundary. Then the resulting heat flow through the two specimens from the hot surface to the cold surface is averaged and recorded [26].

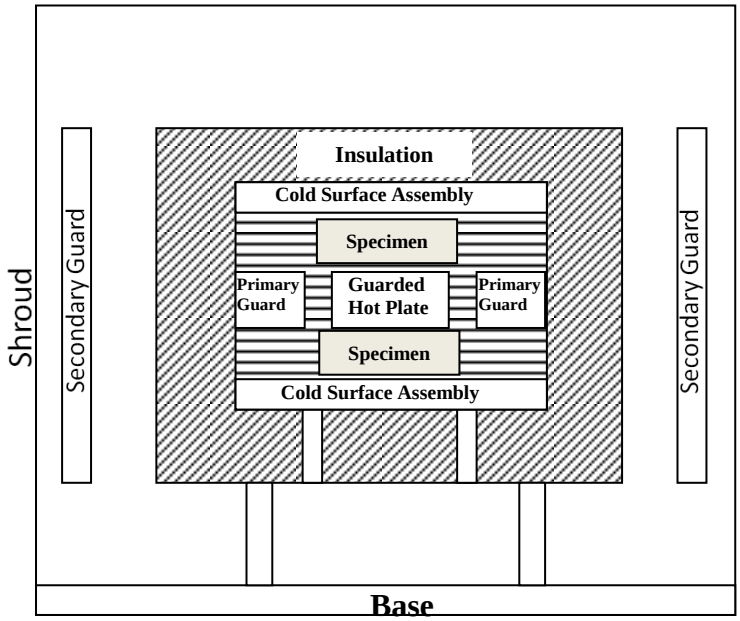

Figure 1.6: General Arrangement of the Mechanical Components of the Guarded-Hot-Plate Apparatus [26].

Deviations from the idealized configurations are, however, still considerable, because of experimental defects such as the non-homogeneities of specimens, the temperature differences between the metered section and the guard as well as the temperature differences between the outer edge of the assembly and the surrounding controlled environment etc. All these heat propagating routes would result in lateral heat flow within the apparatus; and subsequently the heat flow through specimens along the direction of temperature gradient is not exactly equal to the heat flow supplied to the metered section under consideration (Figure 1.7).

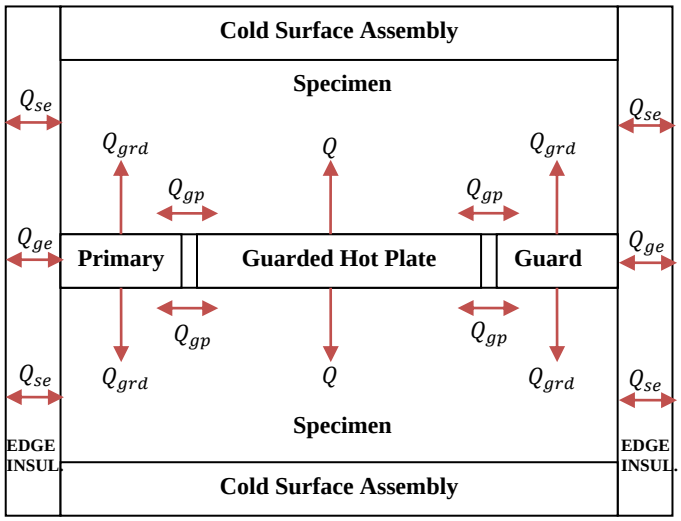

Figure 1.7: Illustration of Idealized Heat Flow in a Guarded-Hot-Plate Apparatus.

Therefore, to measure the materials with better accuracy, the apparatus has to be optimized for operation. Basically, the linear dimension of the metered section shall be ensured; and the temperature along the surface plate of the hot surface assembly in the lateral direction should be constant with less than 2% of the temperature difference across the specimen. The gap between the metered section and the primary guard is necessary with same distance not more than 5% of the metered section area to provide a lateral thermal resistance. More specific configurations are recommended in the ASTM C177 standard [26].

The temperature is monitored at each surface based on thermocouples readings. The heat transferred through specimens is equal to the power supplied to the metered section. The steady-state is achieved when temperature and voltage readings become steady. Then the thermal conductivity is calculated using [27]:

$$K = \frac{pow}{[Lt * (T_m - T_a)]} \quad (27)$$

Where:

Pow: *Power supplied to the main heater*

Lt: *Total specimen thickness (twice the single specimen thickness, L)*

T_m: *Temperature of the main heater*

T_a: *Temperature of the auxiliary heat*

Though experimental measurement could offer direct illustrations, the operation is actually expensive and time consuming. Additionally, the experimental error is considerable, not only because the thermal properties of fibrous materials are sensitive to many environmental factors, such as temperature, moisture and pressure etc., but also the results may vary significantly from one operation to another with different apparatus specifications. Thus, it is necessary to periodically calibrate such equipment.

2. Lattice Boltzmann Method (LBM)

2.1. Introduction

2.1.1. Evolution Equation

Lattice Boltzmann model (LBM) is a modern numerical scheme in simulating fluid flows through media. It has achieved remarkable success, as it has been proved to be stable, accurate and computationally efficient compared with convention approaches [28, 29]. A lot of work has been done so far by applying the method to solve problems related to isothermal fluids with single-component in single phase or single-component in multiphase or

multicomponent in multiphase. Here, the terminology component is referred to base on the phase of the chemical constituents. A single component multiphase system involves the liquid and vapor phases is considered. The number of relevant papers published has been growing exponentially during the past decade, as shown in Figure 2.1. Particularly, LBM is effective on applications involving interfacial dynamics and complex boundaries because of the ease of implementations of multiple component/phase interactions and complex boundary conditions with difficult geometries such as fibrous media with porous structure [28].

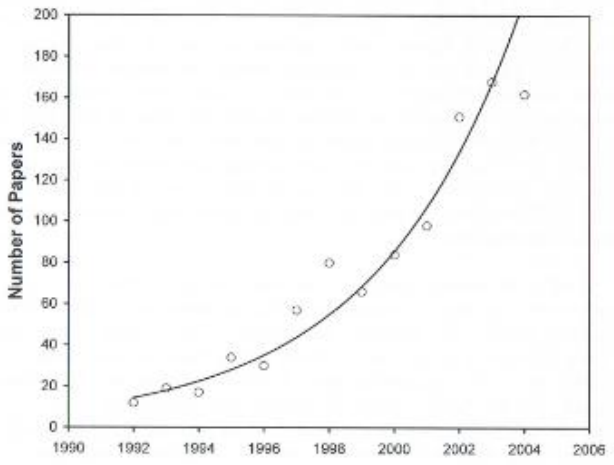

Figure 2.1: Number of Papers with "Lattice Boltzmann" Web of Science Database 1992-2004. Solid Line is Fitted Exponential Growth Curve [28].

Lattice Boltzmann equations evolved based on the kinetic theory, in which a dilute gas is considered as consisting of interacting particles with elastic collisions among one another.

$$\partial_t f + (\boldsymbol{\xi} \cdot \nabla) f = \Omega(f) \tag{28}$$

$$\Omega(f) = -\tau^{-1}(f - f^{eq}) \tag{29}$$

Where:

f: *Single particle density distribution function*

$\boldsymbol{\xi}$: *Microscopic velocity*

Ω: *Collision term*

τ: *Single-relaxation time*

f^{eq}: *Equilibrium distribution of particle density*

Ludwig Boltzmann, who came up with the notions of gases and the atomic theory of matter, proposed an essential and appropriate statistical treatment of so many interacting particles. The mechanism of the treatment is that the evolution of the single-particle density distribution in a fluid is simply encapsulated with notions of streaming in space and collision interactions. In streaming, the direction specific densities, f_α, is moved to the nearest neighbor lattice nodes; and the relaxation towards to the local equilibrium, f^{eq}, because of the collisions occurred afterwards. Thus, the two-step evolution equation can be expressed as: [28, 30-34]

$$f_\alpha(\boldsymbol{x} + \boldsymbol{e}_\alpha\delta_t, t + \delta_t) - f_\alpha(\boldsymbol{x}, t) = -\frac{1}{\tau}(f(\boldsymbol{x}, t) - f_\alpha^{eq}(\boldsymbol{x}, t)) \tag{30}$$

Where:

$\boldsymbol{x}$: *Node position*

α: *Direction index of velocity,* $\alpha = 1,2,3, \ldots$

$\boldsymbol{e_\alpha}$: *Discrete velocity*

t: *Real time*

δ_t: *Tme step*

In the above equation, the LH side:

$$f_\alpha(\boldsymbol{x} + \boldsymbol{e_\alpha}\delta_t, t + \delta_t) - f_\alpha(\boldsymbol{x}, t) \tag{31}$$

is the streaming step and the RH side:

$$-\frac{1}{\tau}\Big(f(\boldsymbol{x}, t) - f_\alpha^{eq}(\boldsymbol{x}, t)\Big) \tag{32}$$

is the collision term.

Applying the lattice algorithm has greatly reduced the computational cost of Boltzmann's original concept, Boltzmann kinetic equation, which is the evolution equation for a continuous one-body distribution function. All details of the molecular motion are simplified into those that are strictly needed to represent the hydrodynamic behavior at the macroscopic scale. Specifically, real fluids are reproduced by confining the particle spatial positions to the nodes and discretizing continuum into distinct finite time steps.

2.1.2. D2Q9 Lattice Boltzmann Model

Two-dimensional nine-speed (D2Q9) LBM (Figure 2.2) is one of the most popular model. It is developed based on a two-dimensional five-speed (D2Q5) Lattice Boltzmann model proposed by Qian et al [33]. The model simply considers that all interacting particles have one unique particle mass propagating into 9 possible discrete velocities (i.e. $e_\alpha,\ \alpha = 1,2,\dots,9$) with 3 magnitudes. [28]. The velocity magnitude of e_1, e_3, e_5, e_7 is 1 lattice unit per time step; and the velocity magnitude of e_2, e_4, e_6, e_8 is $\sqrt{2}$ lattice unit per time step.

The LBM is intrinsically a mescoscopic approach based on the evolution of statistical distribution of lattices [30].As shown in the Figure 2.3, the frequency of occurrence for each specific discrete velocity involved in the D2Q9 model is represented by the corresponding

density distribution function, f_α. For a simple understanding, the density distribution function can be considered as the frequency of occurrence in a typical histogram.

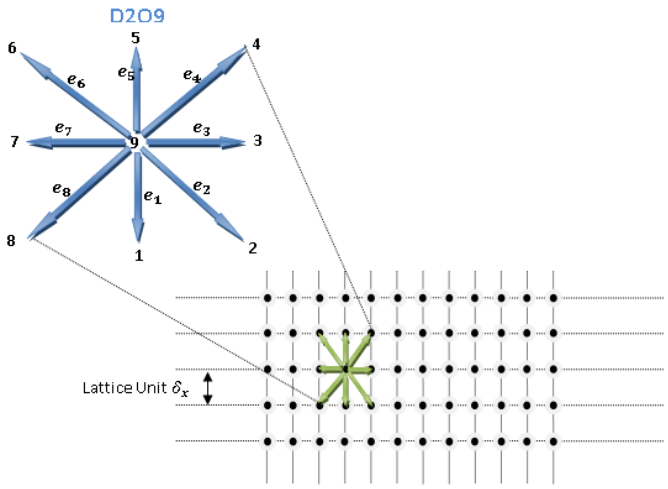

Figure 2.2: Schematic of D2Q9 Lattice Boltzmann Model with 9 Discrete Velocities.

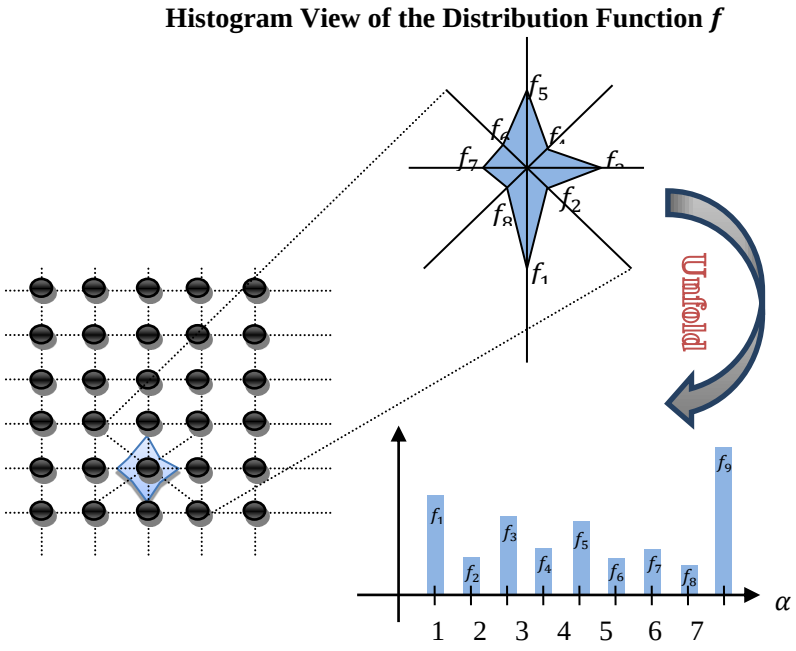

Figure 2.3: The Schematic of the Histogram View of the Distribution Function f.

Each discrete velocity, e_α with specific direction and magnitude is then represented with their corresponding coordinates:

$$\boldsymbol{e_\alpha} = \begin{cases} (0,0) & \alpha = 9 \\ \left(cos\left[\frac{(\alpha-1)\pi}{2}\right], sin\left[\frac{(\alpha-1)\pi}{2}\right]\right)c & \alpha = 1,3,5,7 \\ \sqrt{2}\left(cos\left[\frac{(\alpha-5)\pi}{2}+\frac{\pi}{4}\right], sin\left[\frac{(\alpha-5)\pi}{2}+\frac{\pi}{4}\right]\right)c & \alpha = 2,4,6,8 \end{cases} \quad (33)$$

Where c is the characteristic speed depending on the value of lattice constant,δ_x, and time step, δ_t, (i.e., $c = \frac{\delta_x}{\delta_t}$). The characteristic speed is always a constant value [30, 31]. With a larger value taken, the better accuracy could be obtained; however, the computational costs would increase exponentially. [31, 32]

By replacing in the values of α, the discrete velocity, e_α, can then be simplified as:

$$\boldsymbol{e_\alpha} = \begin{cases} (0,0) & \alpha = 9 \\ (\pm 1,0) * c, (0, \pm 1) * c & \alpha = 1,3,5,7 \\ (\pm 1, \pm 1) * c & \alpha = 2,4,6,8 \end{cases} \quad (34)$$

The equilibrium distribution function f^{eq} is given by:

$$f^{eq} = \omega_\alpha \rho[1 + \frac{3\boldsymbol{e_\alpha} \cdot \boldsymbol{u}}{c^2} + \frac{9}{2}\frac{(\boldsymbol{e_\alpha} \cdot \boldsymbol{u})^2}{c^4} - \frac{3}{2}\frac{u^2}{c^2}] \quad (35)$$

where:

$$\omega_\alpha = \begin{cases} \frac{4}{9} & \alpha = 9 \\ \frac{1}{9} & \alpha = 1,3,5,7 \\ \frac{1}{36} & \alpha = 2,4,6,8 \end{cases} \quad (36)$$

Therefore, the macroscopic fluid density, ρ, velocity, u, and temperature, T, can be calculated by

$$\rho = \sum_{\alpha=1}^{9} f_\alpha \quad (37)$$

$$\boldsymbol{u} = \frac{1}{\rho} \sum_{\alpha=1}^{9} f_\alpha \, \boldsymbol{e_\alpha} \quad (38)$$

$$\frac{\rho DRT}{2} = \sum_{\alpha=1}^{9} \frac{(\boldsymbol{e_\alpha} - \boldsymbol{u})^2 f_\alpha}{2} \quad (39)$$

Where:

D: Dimension

R: Gas constant

2.1.3. Applications in Simulating Thermal Transmissions

Not only the Lattice Boltzmann method was successful in simulating fluid flows, it is also broadly applied for solving heat transfer problems as a competent approach. R. Chaabane et al. modeled the thermal conduction effect in a single-component rectangular slab based on specified heat flux and temperature boundary conditions with the D2Q9 model. The top and

bottom bounds were set to be insulated; and isothermal boundary condition was applied on the left and right bounds. The higher-order velocity terms and the temperature evolution drawn from the density distribution function were then compared with the results calculated with finite volume method. An agreement was obtained between the two models. The dimensionless relaxation time towards the equilibrium distribution applied in the model was determined to be a function of the thermal conductivity, *K*, the lattice velocity, c, and the time step, δ_t, with the following relation. [35]

$$\tau = \frac{3K}{c^2} + \frac{\delta t}{2} \qquad (40)$$

Generally, there are two conventional categories of approaches on simulating the transportation of heat transfer with LBM: the multispeed approach and the passive-scalar approach. The former approach is to obtain the temperature evolution equation at the macroscopic level with additional speeds involved. Moreover, it is inevitable to include the high-order velocity terms in the equilibrium distribution, which would increase the computational costs. The approach has been proved to be theoretically feasible; however, it is very instable and the temperature variation was limited to a narrow range. Subsequently, the approach was not apt to be applied in a broader scale. The latter approach was dealing with models with negligible effects of viscous heat dissipation and compression work done by the pressure. It simulates temperature evolution with a separated distribution function isolated with the density distribution. The approach presented better numerical stability and accuracy than the multispeed approach. [31]

The enhanced Lattice Boltzmann method that is based on the second approach was therefore, adopted here for the numerical model of the heat transfer across nonwoven composites.

2.2. Thermal Lattice Boltzmann Model

2.2.1. Evolution Equations, Macroscopic Temperature and Heat Flux

The D2Q9 thermal model used in this study is the one specifically designed for simulating thermal conduction through bi-component/phase porous media by Xiaoyi He et al. A new variable, the energy density distribution function, g, calculated from the density distribution, f, was proposed; so that the temperature change and heat flux distribution in nonwoven composites are simulated. The composites are considered to be, in this approach, with two components including fibers and gas with complex interactions because of the randomly distributed porous structure. In this model only thermal conduction is considered. It is realistic to neglect convection when the pore sizes are small, and no overall air motion is allowed. In addition, radiation could be also ignored at ambient temperature. Then the energy equations describing thermal conduction through fibrous structures without internal heat generation are [30, 31]

$$\left(\rho C_p\right)_f \left(\frac{\partial T}{\partial t}\right) = k_f \nabla^2 T \qquad (41)$$

$$\left(\rho C_p\right)_g \left(\frac{\partial T}{\partial t}\right) = k_g \nabla^2 T \qquad (42)$$

The internal energy density distribution function was determined by the squared difference between microscopic velocity, $\boldsymbol{\xi}$, and macroscopic velocity, $\boldsymbol{u}$, and the density distribution. [31]

$$g = \frac{(\boldsymbol{\xi} - \boldsymbol{u})^2}{2} f \tag{43}$$

The discrete internal energy density equilibrium distribution,g^{eq} corresponding to f^{eq} is given by:

$$g_9^{eq} = -\frac{2\rho\epsilon}{3}\frac{\boldsymbol{u}^2}{c^2} \tag{44}$$

$$g_{1,3,5,7}^{eq} = \frac{\rho\epsilon}{9}[\frac{3}{2} + \frac{3}{2}\frac{\boldsymbol{e_\alpha}\cdot\boldsymbol{u}}{c^2} + \frac{9}{2}\frac{(e_\alpha\cdot\boldsymbol{u})^2}{c^4} - \frac{3}{2}\frac{\boldsymbol{u}^2}{c^2}] \tag{45}$$

$$g_{2,4,6,8}^{eq} = \frac{\rho\epsilon}{9}[3 + 6\frac{\boldsymbol{e_\alpha}\cdot\boldsymbol{u}}{c^2} + \frac{9}{2}\frac{(\boldsymbol{e_\alpha}\cdot\boldsymbol{u})^2}{c^4} - \frac{3}{2}\frac{\boldsymbol{u}^2}{c^2}] \tag{46}$$

Where:

ϵ: Internal Energy

It can be obtained with the following equation:

$$\epsilon = DRT/2 \tag{47}$$

Since there is no macroscopic fluid velocity ($u = 0$) in the whole system, thus, the equilibrium distribution could be simplified as the following function of the temperature

$$\begin{cases} g_9^{eq} = 0 \\ g_{1,3,5,7}^{eq} = \frac{1}{6}T \\ g_{2,4,6,8}^{eq} = \frac{1}{12}T \end{cases} \tag{48}$$

In general, the streaming and collision terms of LBM in both solid and fluid phases can be expressed as [30, 31]:

$$g_\alpha(\boldsymbol{x} + \boldsymbol{e_\alpha}\delta_t, t + \delta_t) - g_\alpha(\boldsymbol{x}, t) = -\frac{1}{\tau}(g_\alpha(\boldsymbol{x}, t) - g_\alpha^{eq}(\boldsymbol{x}, t) \tag{49}$$

Thus, the temperature and heat flux then can be calculated by the following summations:

$$T = \sum_{\alpha=1}^{9} g_\alpha \tag{50}$$

$$q = (\sum_{\alpha=1}^{9} \boldsymbol{e_\alpha} g_\alpha)\frac{\tau - 0.5}{\tau} \tag{51}$$

Once the temperature profile is generated, the effective thermal conductivity K_{eff}, can be calculated for the steady state heat flux through the media cross-section area, dA, held between the temperature differences, ΔT, over a distance L. [30, 36]

$$K_{eff} = \frac{L \cdot \int q \cdot dA}{\Delta T \int dA} \tag{52}$$

Due to the complex structural boundary conditions, the heat transfer for each component has to be considered separately in term of the relaxation time, τ, which is determined by the thermal conductivity of each phase and defined as [30, 32]

$$\tau_f = \frac{3}{2}\frac{k_f}{(\rho c_p)_f \cdot c^2 \delta_t} + 0.5 \quad (53)$$

$$\tau_g = \frac{3}{2}\frac{k_g}{(\rho c_p)_g \cdot c^2 \delta_t} + 0.5 \quad (54)$$

Where:

ρ: Density of each component

c_p: The specific heat of each component

2.2.2. Continuity on Interface

Meanwhile, the continuity constraints have to be satisfied at the inter-phase surfaces with equal temperature and heat flux under assumptions that: No phase change and negligible contact thermal resistance between fibers. In order to assure the continuity satisfaction, the specific heat for fiber phase $(\rho C_p)_f$ is artificially set to be identical to the counterpart in gas phase $(\rho C_p)_g$, while maintaining the conductivity of each component as its real value. The approach is called 'pseudo-solid-specific heat' method and has been proved valid with negligible error when solving conjugate heat transfer problems [37]. The lattice speed, c, could be theoretically any positive value only to insure the values of $\in (0.5,2)$. Here the speed is defined as $c = \sqrt{3RT_{avg}}$ in the numerical model [31, 32].

Equal temperature:

$$T_{f,int} = T_{g,int} \quad (55)$$

And Equal heat flux through the interface:

$$k_f \frac{\partial T}{\partial n}|_{f,int} = k_g \frac{\partial T}{\partial n}|_{g,int} \tag{56}$$

Then, the treatment can be implemented with the following equations:

$$\tau_f = \frac{3}{2}\frac{k_{\boldsymbol{f}}}{(\rho c_p)_{\boldsymbol{g}} \cdot c^2 \delta_t} + 0.5 \tag{57}$$

$$\tau_g = \frac{3}{2}\frac{k_{\boldsymbol{g}}}{(\rho c_p)_{\boldsymbol{g}} \cdot c^2 \delta_t} + 0.5 \tag{58}$$

2.3.3. Boundary Condition Treatment

Insulated and isothermal boundary treatments on four bounds are applied in this work. The isothermal boundary treatment is applied on the left and the right bounds with temperature T_1 and T_2, where $T_1 > T_2$; and the insulated boundary treatment is applied on the top and bottom bounds as presented in the Figure 2.4. And the treatment follows the bounce-back rule of the non-equilibrium distribution, as proposed by Zou and He, assuming that the bounceback condition holds in the direction normal to the boundaries: [38]

$$g_\alpha - g_\alpha^{eq} = (g_\beta - g_\beta^{eq}) \tag{59}$$

Where the subscripts α and β represent two opposite directions. Zou and He boundary condition simulation has better numerical accuracy and ease of implementation, particularly in 2D models; however, the weak point is deficient numerical stability. [39]

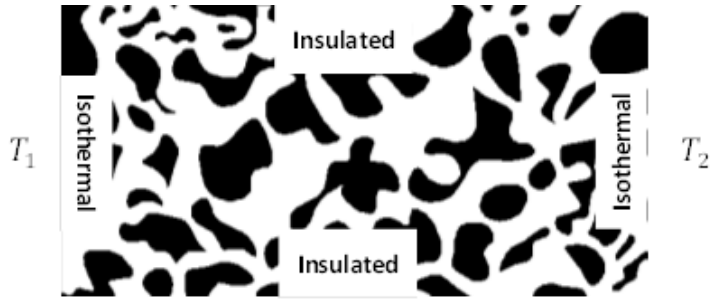

Figure 2.4: Schematic of a Porous Media with Isothermal and Insulated Boundary Treatments.

2.3.3.1. Dirichlet (Temperature) Boundaries

Taking the left boundary of the composite as an example to illustrate the isothermal boundary condition, after streaming the energy density distribution in six directions, i.e. $\alpha = 1, 5, 6, 7, 8, 9$, are updated with the particles inside of the system; however, the rest three dictions, i.e.$\alpha = 2, 3, 4$, are unknown (Figure 2.5). Additionally, heat flux on the boundary is also unknown. Therefore, four equations are necessary to solve all the four unknown factors.

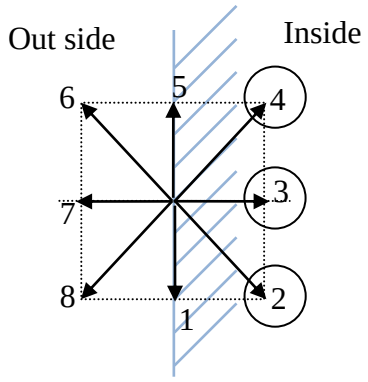

Figure 2.5: Unknown Direction-specific Densities g_2, g_3, g_4 after Streaming at Left Surface.

As introduced in the equation (50) and (51), the temperature on the left face, T_1 has been constrained as constant and expressed as the sum of the energy density distribution:

$$T_1 = g_1 + g_2 + g_3 + g_4 + g_5 + g_6 + g_7 + g_8 \quad (60)$$

The macroscopic heat flux can be specified both in the x direction and y direction:

$$q_x = \frac{\tau - 0.5}{\tau} * (g_4 + g_3 + g_2 - g_6 - g_7 - g_8) \quad (61)$$

$$q_y = \frac{\tau - 0.5}{\tau} * (g_4 + g_5 + g_6 - g_2 - g_1 - g_8) \quad (62)$$

There is no heat flux on the y direction on the left bound where high temperature T_1, is applied, i.e. $q_y = 0$

Finally, the bounceback condition is applied on the energy density distribution functions perpendicular to the left face, i.e.

$$g_3 - g_3^{eq} = (g_7 - g_7^{eq}) \quad (63)$$

Where the equilibrium state can be calculated by the local temperature, and found out to be:

$$g_3^{eq} = g_7^{eq} \quad (64)$$

Therefore, condition:

$$g_3 = g_7 \quad (65)$$

is applied on the bound.

After solving the four equations, the four unknown factors can then be expressed as:

$$g_2 = \frac{T_1 - 2g_1 - 2g_7 - 2g_8}{2} \quad (66)$$

$$g_3 = g_7 \tag{67}$$

$$g_4 = \frac{T_1 - 2g_5 - 2g_6 - 2g_7}{2} \tag{68}$$

$$q_x = \frac{T_1 - g_1 - g_5 - 2g_6 - 2g_7 - 2g_8}{a} \tag{69}$$

Where:

$$a = \frac{\tau - 0.5}{\tau} \tag{70}$$

Due to the symmetry, the same approach can be applied on the right boundary, where the constant temperature, T_2, is constrained.

And the result is:

$$g_6 = \frac{T_2 - 2g_3 - 2g_4 - 2g_5}{2} \tag{71}$$

$$g_7 = g_3 \tag{72}$$

$$g_8 = \frac{T_2 - 2g_1 - 2g_2 - 2g_3}{2} \tag{73}$$

And;

$$q_x = \frac{g_1 + 2g_2 + 2g_3 + 2g_4 + g_5 - T_2}{a} \tag{74}$$

2.3.3.2. Von Neumann (Heat Flux) Boundaries

Regarding the insulated boundary treatment for the top and bottom surfaces, they follow the Neumann boundary condition and impose the boundary temperature gradient in the y-direction to be zero, i.e. $q_y = 0$, so that there is no heat flux leaking from the boundaries. A specular reflection treatment, which is a mirror-like reflection of waves, is implemented to prevent heat flux from leaking along the surfaces. Particles propagating with velocities towards the insulation boundaries, i.e. top and bottom faces in the model, are reflected back into the structure following the law of reflection. Numerically, the reflection is described by the equation: [28, 38]

$$g_\alpha = g_\gamma \tag{75}$$

Where the subscripts α and γ represent the two directions before and after specular reflection with equal incident angles and reflected angles.

The insulated boundary condition is closely related to the isothermal treatment. Similarly, after streaming, there are three unknown energy densities in directions of $1, 2, 8$, and have to be calculated with the other six direction values (Figure 2.6).

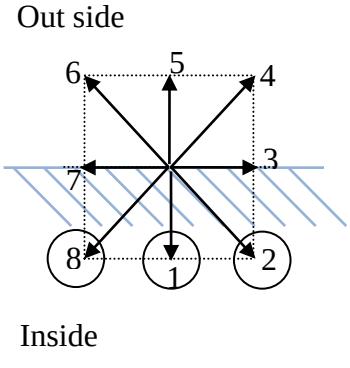

Figure 2.6: Unknowns (Circled) Energy Densities after Propagating at the Top Surface.

According to the bounceback treatment proposed, here take the top bound as example, equations that are known are:

$$q_y = \frac{\tau - 0.5}{\tau} * (g_4 + g_5 + g_6 - g_2 - g_1 - g_8) = 0 \quad (76)$$

$$g_1 = g_5 \quad (77)$$

Then the following relationship can be obtained,

$$g_2 + g_8 = g_4 + g_6 \quad (78)$$

Subsequently the specular reflection treatment the following deduction can be applied

$$g_2 = g_4 \quad (79)$$

$$g_8 = g_6 \quad (80)$$

Due to the symmetry, similar approach is applied on the bottom bound. By solving equations with known factors the system can be reduced to

$$g_5 = g_1 \quad (81)$$

$$g_4 = g_2 \quad (82)$$

$$g_6 = g_8 \quad (83)$$

3. Results and Discussion

3.1. Benchmarks

3.1.1. Sing-phase Lattice Boltzmann Model

The temperature evolution from transient state to the steady state of a solid slab with single component, single-phase was simulated with the enhanced LBM. In order to assess its accuracy, comparison was made with the result from Matlab Partial Differential Equation Tool Box™ (PDE Tool Box), which solves the energy equations with finite element algorithm. However, the tool box is only workable for materials with simple geometries, thus, the tool box is not applied to valid the bi-component models.

The initial conditions and boundary treatments of the slab are set as follow:

Initially, the slab is assumed having same temperature, T_0, which is considered as the room temperature, such as:

$$T(x,y)|_{t=0} = T_0 \tag{84}$$

Higher temperature T_1 ($T_1 > T_0$) is applied on the face where $x = 0$, such as:

$$T(0,y)|_{t=0} = T_1 \tag{85}$$

And the lower temperature T_2 , which is equal to T_0 is then applied on the rest three surfaces remaining the initial condition, such as:

$$T(L,y)|_{t=0} = T(x,0)|_{t=0} = T(x,W)|_{t=0} = T_2 \tag{86}$$

Where L is the thickness of the slab, i.e. the distance between two different temperature levels and W is the width (Figure 3.1).

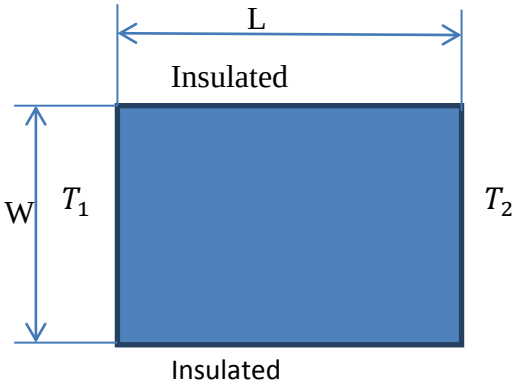

Figure 3.1: Schematic of a Solid Slab with Single-component, Single-phase.

Isothermal treatment is maintained on the bounds at $x = 0\ and\ x = L$ in a Dirichlet boundary condition and insulated treatment for the other two bounds with a Neumann boundary condition.

$$T(0, y)|_{t>0} = T_1 \tag{87}$$

$$T(L, y)|_{t>0} = T_2 \tag{88}$$

$$\frac{\partial T}{\partial x}|_{y=0,t>0} = \frac{\partial T}{\partial x}|_{y=W,t>0} = 0 \tag{89}$$

The temperature profile and heat flux distribution at steady state are simulated with the above mentioned configurations (Figure 3.2); and the results are plotted in 2-D and 3-D modes (Figure 3.3):

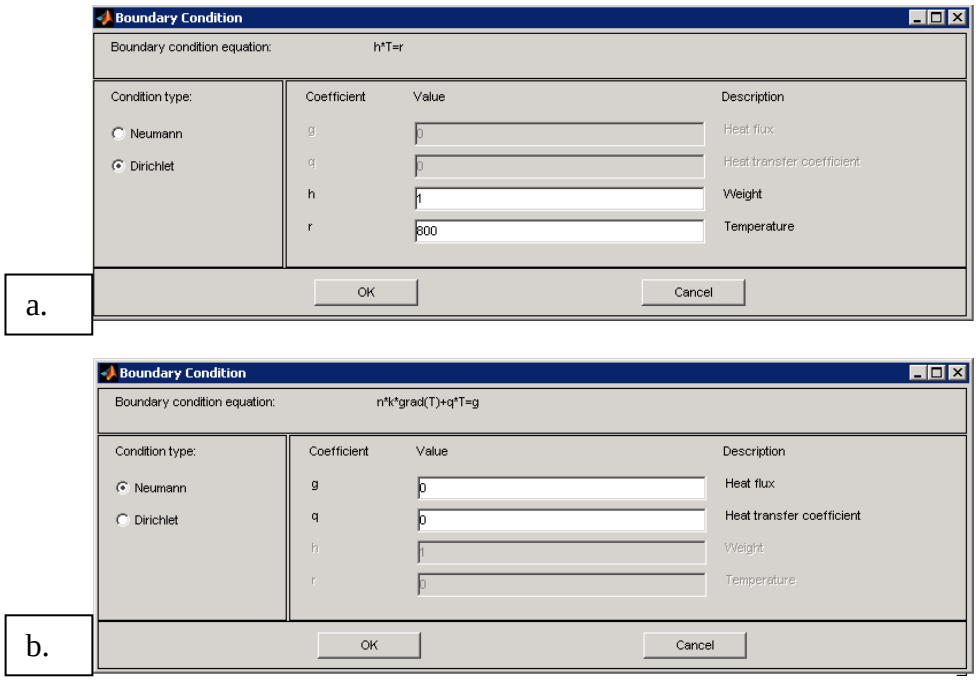

Figure 3.2: Treatments on Single Component Slab with PDE Tool Box: a. Boundary Condition on the Left Bound with $T_1 = 800\ K$; b. Boundary Condition on the Top and Bottom Surface with Neumann Treatment.

The temperature profile and heat flux distribution at steady state obtained from the LBM are plotted in 2-D and 3-D (Figure 3.4). Here, the steady state is considered to be achieved when the temperature difference between two consecutive time steps is smaller than $10^{-6}\ K$ [35].

a.

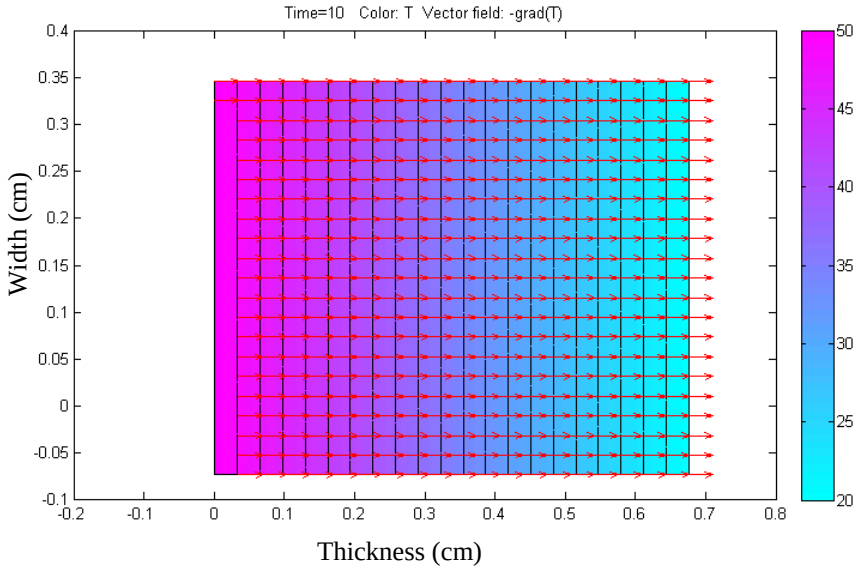

b.

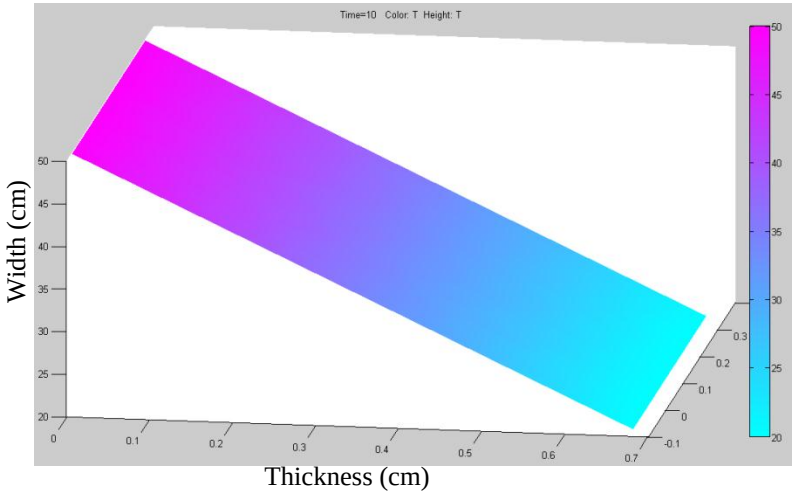

Figure 3.3: Temperature Profile and Heat Flux Resulting from PDE Tool Box.

a.

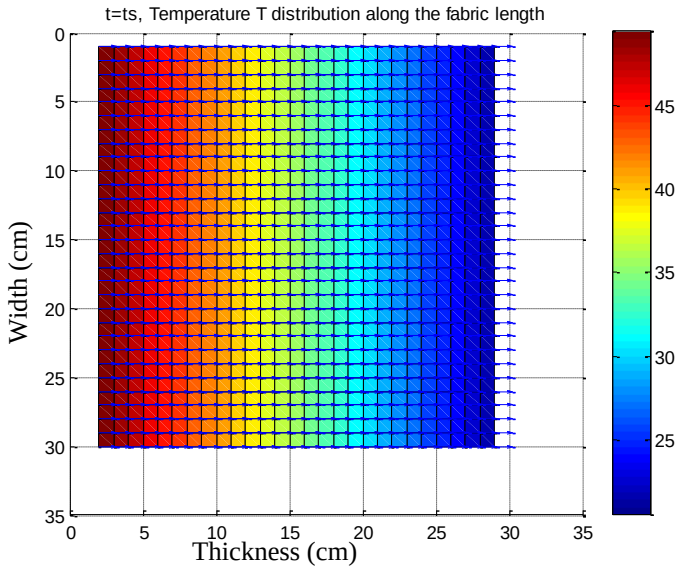

b.

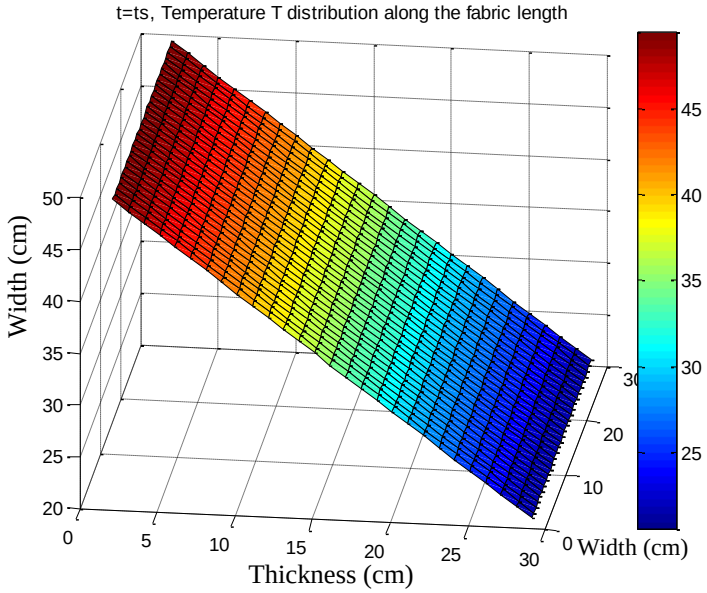

Figure 3.4: Temperature Profile and Heat Flux Calculated with LBM in a. 2-D and b.3-D Contour.

When the steady state has been achieved with pure thermal conduction, the temperature profile is linearly distributed along the slab thickness between T_1 and T_2. The speed of

achieving steady state is controlled by the dimensionless relaxation time which is determined by the thermal conductivity of the component.

$$T_{t+\delta t} - T_t < 10^{-6}\ (K) \tag{90}$$

A close agreement between the results solved with LBM and finite element methods is obtained. The temperature evolution on two randomly selected nodes within the structure is recorded for the first 1000 time steps δt and plotted in Figure 3.5. Temperature vibratingly rises with increasing time until an asymptotic value is reached. Before achieving this maximum value, the whole system is in a transient state.

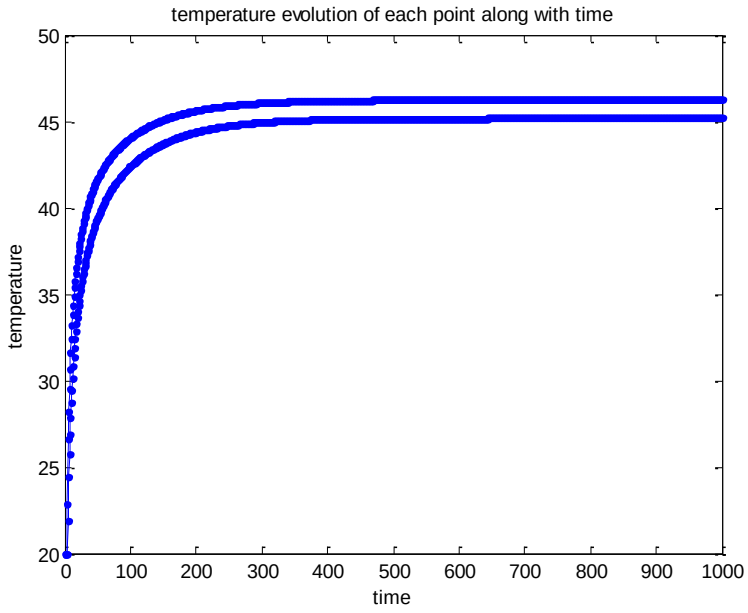

Figure 3.5: Temperature Evolution at Two Randomly Selected Nodes.

The temperature contours at six different time step, ($\delta_t = 50, 100, 200, 300, 500, 1000$) are plotted to explicitly clarify the temperature evolution procedure from a transient state to the steady state (Figure 3.6).

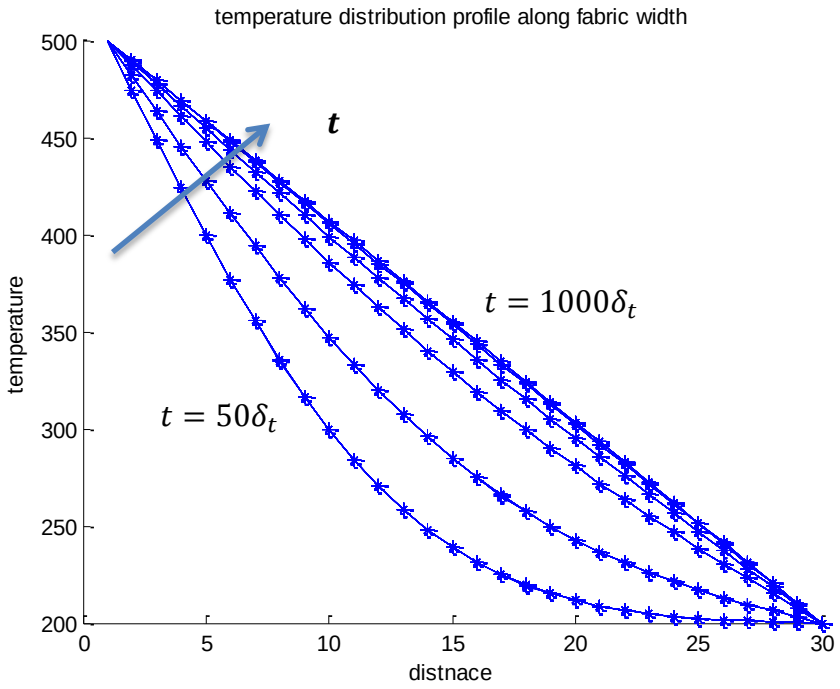

Figure 3.6: Temperature Distribution Evolves from Transient States to Steady State at Time Steps $\delta_t = 50,100,200,300,500,1000$.

3.1.2. Two-phase Lattice Boltzmann models

The two simple heat transfer modes with two-components are the parallel mode and the series mode as shown in the Figure 3.7. Two components with different heat conductivities ($K_1 < K_2$) are arranged parallel along the media thickness and vertically aligned one another in the series mode.

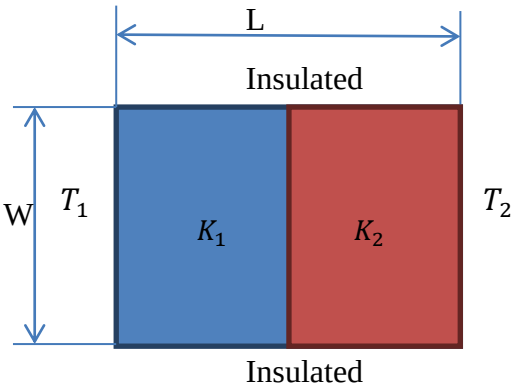

(a) Series mode

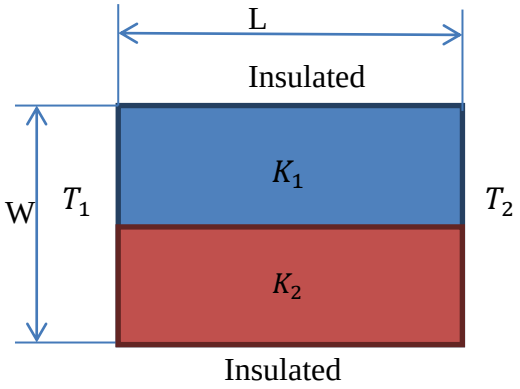

(b) Parallel Mode

Figure 3.7: Two Simple Modes with Two-components: a. Series Mode; b. Parallel Mode.

Boundary conditions similar to those for the single-component model are applied here to the two modes. The modes are simulated with the enhanced Lattice Boltzmann Method. The resulting effective thermal conductivity is compared with the theoretical solutions, which are given by:

For the Series Mode:

$$K_{eff} = \frac{1}{(\frac{1}{2K_1} + \frac{1}{2K_2})} \tag{91}$$

And for the Parallel Mode:

$$K_{eff} = \frac{(K_1 + K_2)}{2} \tag{92}$$

Calculations obtained with LBM are presented in Table 3.1. High level error may occur when K_2 is much greater than K_1. This is caused by the large value of relaxation time τ for fiber phase, which has severely exceeded the proposed range ($\tau = 8.1396 \gg 2$).

Table 3.1: Effective Thermal Conductivities of Theoretical Solution and LB Simulation.

$\mathbf{K_1 : K_2}$	**Parallel Mode**		**Series Mode**	
	Estimated $(\boldsymbol{W.m^{-1}.K^{-1}})$	**Calculated** $(\boldsymbol{W.m^{-1}.K^{-1}})$	**Estimated** $(\boldsymbol{W.m^{-1}.K^{-1}})$	**Calculated** $(\boldsymbol{W.m^{-1}.K^{-1}})$
1:2	1.5	1.34	1.333	1.328
1:5	3.0	2.99	1.667	1.660
1:10	5.5	5.65	1.818	1.811
1:20	10.5	10.43	1.9048	1.897
1:50	25.5	22.52	1.961	1.961

Result of comparison indicates an agreement between the theoretical solution and the calculated one. Then the details of each mode are introduced as follow:

3.1.2.1. Series Mode

The temperature profile after the steady state has been achieved is calculated with the LBM and compared with the analytical solution for the series mode, which is given [40]:

$$T(x) = \begin{cases} T_1 - \dfrac{K_2}{K_1 + K_2} * \dfrac{x}{\frac{L}{2}} * \Delta T & 0 \le x \le \dfrac{L}{2} \\ \dfrac{2K_1T_1 - (K_1 - K_2)T_2}{K_1 + K_2} - \dfrac{K_1}{K_1 + K_2} * \dfrac{x}{\frac{L}{2}} * \Delta T & \dfrac{L}{2} \le x \le L \end{cases} \quad (93)$$

The temperature distribution is linearly associated with the distance, x, along media thickness. Figure 3.8 shows the temperature evolution and the comparison between the analytical solution (dark blue stars) and the results from LBM (light blue line). An agreement between the two solutions is obtained to validate the LB model. Meanwhile, by comparing the two graphs (a and b) in the Figure 3.8, it is illustrated that the slope of temperature distribution in each composite is determined by thermal conductivity combination of each component.

The temperature evolution from the transient state to the steady state of two randomly selected nodes in the structure is illustrated in Figure 3.9; and finally, the temperature profile at the steady state is presented in 2D and 3D plots as shown in Figure 3.10, where the effects of thermal conductivity combination influencing slopes of temperature distribution are presented. Heat flux is driven by the temperature gradient between both boundaries.

a.

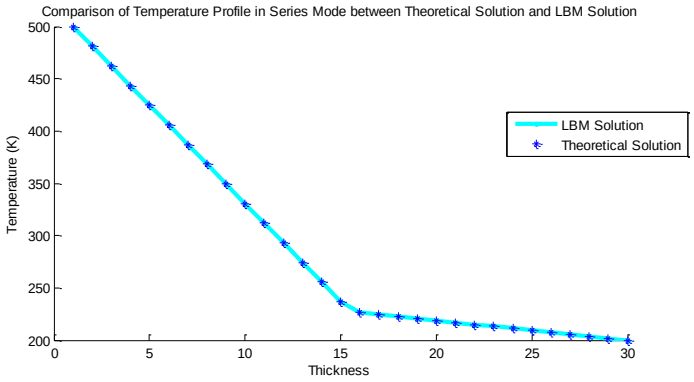

b.

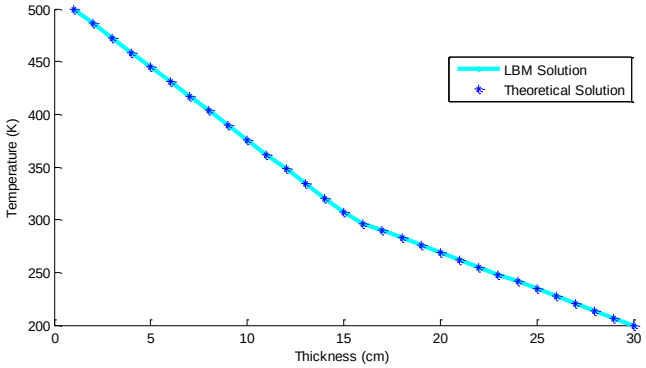

Figure 3.8: Temperature Profile Resulted from Analytical Solution and LBM: a, $K_1 : K_2 = 1 : 5$; b, $K_1 : K_2 = 1 : 2$.

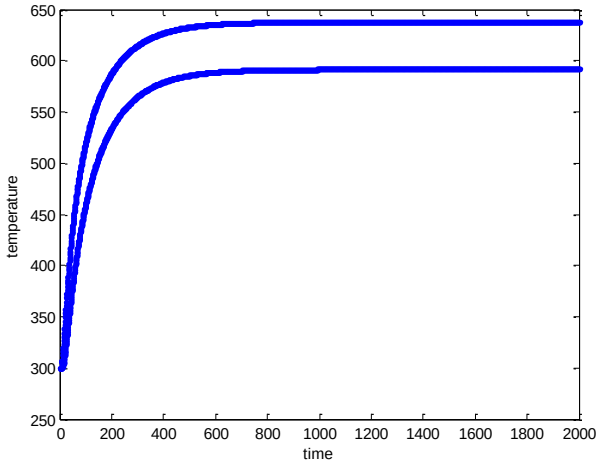

Figure 3.9: Temperature Evolution of Two Randomly Selected Nodes in the Series Mode.

a.

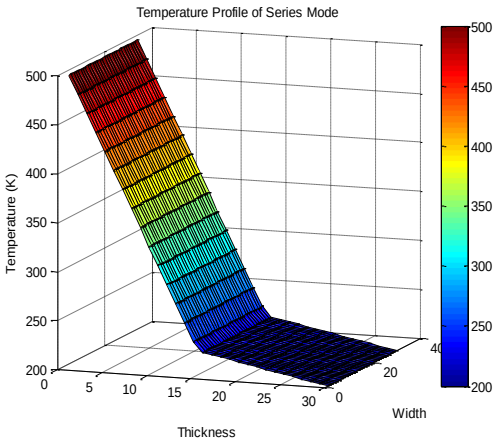

b.

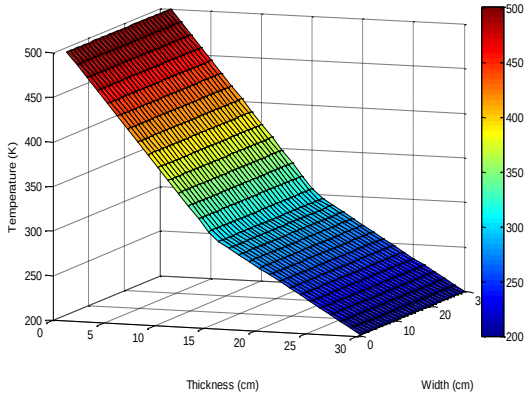

c.

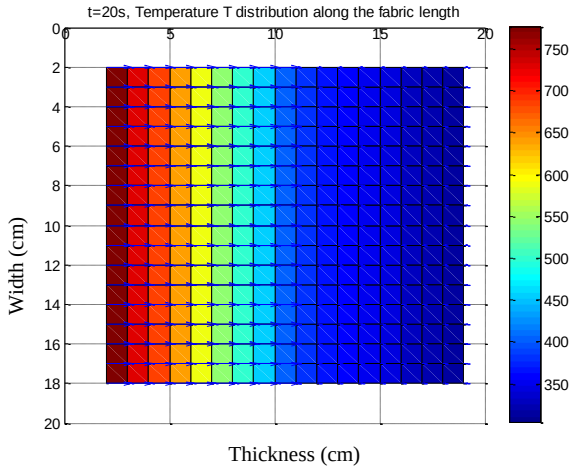

Figure 3.10: Temperature Contours Presented in a. 3D plot ($K_1 : K_2 = 1 : 5$); b. 3D Plot ($K_1 : K_2 = 1 : 2$); c. 2D plot for the Series Mode.

3.1.2.2. Parallel Mode

Parallel heat transfermode was simulated with the same boundary treatments. The results are plotted in the following Figures. Figure 3.11 illustrates the temperature profile in 2D and 3D. When the steady state has been achieved, temperature distribution in both phases has the same linear relationship with the distance, x. However, the temperature evolution is different during the transient states as presented in Figure 3.12. During the transient state, the heat flux is not only flowing along the thickness direction, but also flowing from the component with lower thermal conductivity, K_1, (i.e. higher thermal resistance) to the one with higher thermal conductivity, K_2, (i.e. lower thermal resistance). A comparison of the heat flux between the steady state and the transient state is plotted in Figure 3.13.

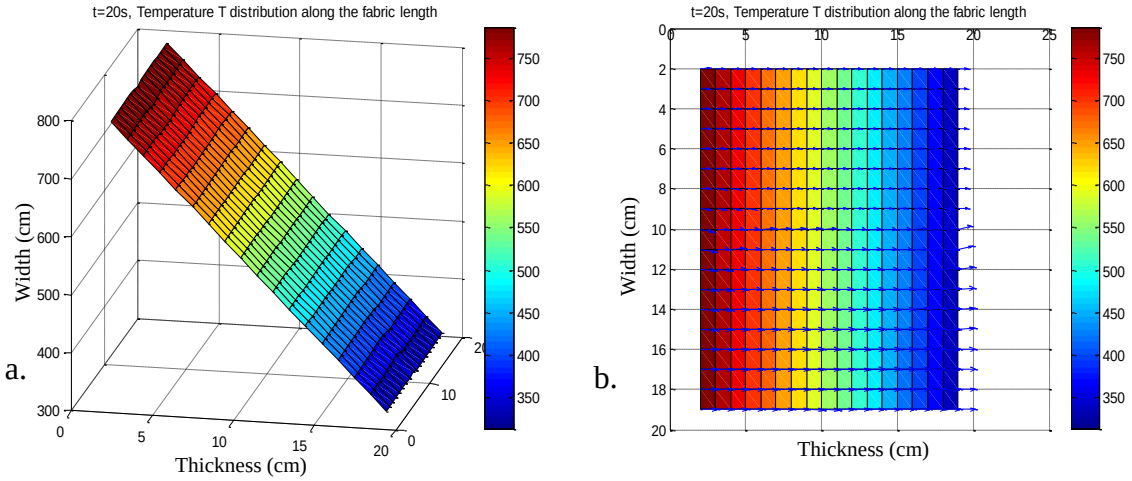

Figure 3.9: Temperature Contour for the Parallel Mode in a. 3D plot and b. 2D plot.

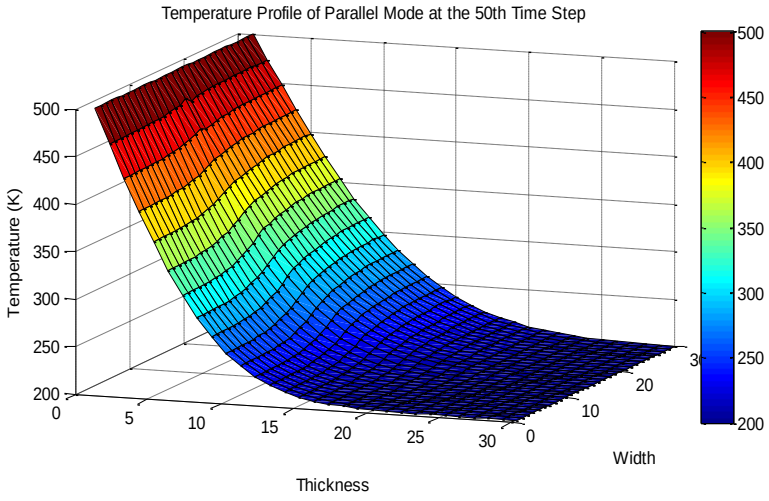

Figure 3.10: Temperature Distribution for the Parallel Mode at the Transient State**.**

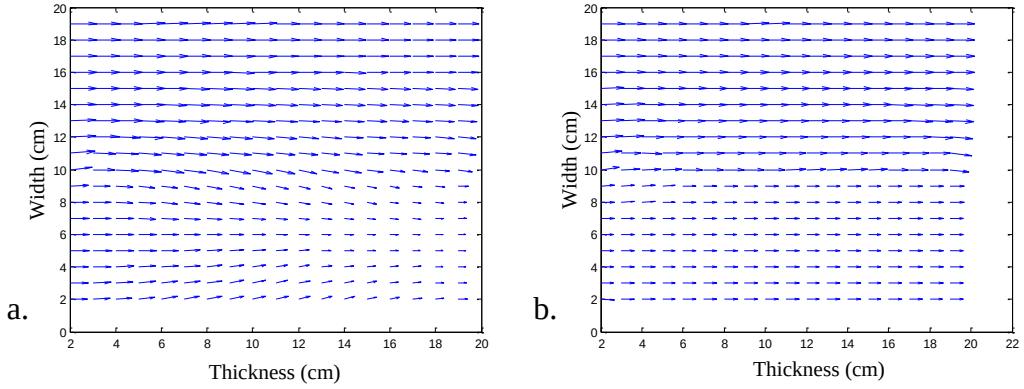

Figure 3.11: Comparison of Heat Flux at a. Transient State and b. Steady State for the Parallel Mode.

3.1.3. Porous media,

3.1.3.1. Comparison with Theoretical Solutions

It is still not enough to validate the enhanced LB model, although the results calculated for the series and parallel modes have shown a perfect agreement with the theoretical results. These two modes are just the most simplified structures of two-component composites when

theoretical approximations are to be made. For all cases, it is impossible for the two components to be distributed in such a uniform pattern; mostly one of them is randomly embedded in the other one (Figure 3.14). Therefore, it is of essence to verify the model in composites with random distribution.

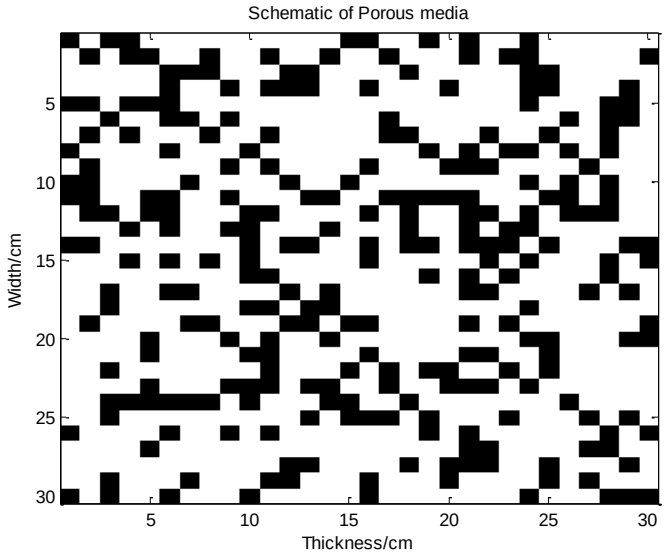

Figure 3.12: Schematic of Porous Media with One Component (30% Solid Volume Fraction) Randomly Distributed in the Other One.

Similar boundary treatments were applied to the bounds of the composite as the one used for the series mode and the parallel mode. It is defined that the material with high thermal conductivity, K_2, is randomly embedded in the component with low thermal conductivity, K_2. Thus, the value of the effective thermal conductivity of composites should be theoretically in between the two values of the series mode and the parallel mode ($K_{se} < K_{eff} < K_p$), such as:

$$\frac{1}{\frac{1}{2K_1}+\frac{1}{2D_2}} < K_{eff} < \frac{(K_1+K_2)}{2} \tag{94}$$

The calculated thermal conductivities for different combinations of $K_1 : K_2$ are compared with estimated values obtained from two theoretical relations (Table 3.2). K_1 remains constant with a value of 1.0 $Wm^{-1}K^{-1}$, while K_2 is varying from 1 to 50 $Wm^{-1}K^{-1}$. [40] Maxwell-Eucken model is a numerical method estimating the thermal conductivities of two-component composites. The model has been proved accurate for simulating the composites with low concentration within the system [41-43]:

$$k_{eff} = \frac{\emptyset_1 K_1 + \emptyset_2 K_2 \frac{3K_1}{K_2 + 2 * K_1}}{\emptyset_1 + \emptyset_2 \frac{3K_1}{K_2 + 2K_1}} \tag{95}$$

Effective medium theory is a similar numerical model based on the effective medium approach as the Maxwell-Eucken method. The model is suitable for heterogeneous structure, with two components randomly distributed, with neither phase being necessarily continuous or dispersed [41-43].

$$\emptyset_1 \frac{K_1 - K_{eff}}{K_1 + 2K_{eff}} + \emptyset_2 \frac{K_2 - K_{eff}}{K_2 + 2K_{eff}} = 0 \tag{96}$$

However, the resulting data from the two theoretical solutions are very rough approximations for the effective thermal conductivity, since both theories are only functions of the thermal conductivity and volume fractions of each component by assuming that the reinforcement/particles are isotropically dispersed in the matrix (Figure 3.15), without taking

the geometrical aspects, such as fiber size and the shape etc., into account. For randomly distributed porous structures, the real value of the thermal conductivity is closely related to the microstructure and the dimensions of reinforcement/particles. Thus, the two theories are inadequate to describe the thermal behavior of fibrous nonwoven composites [44].

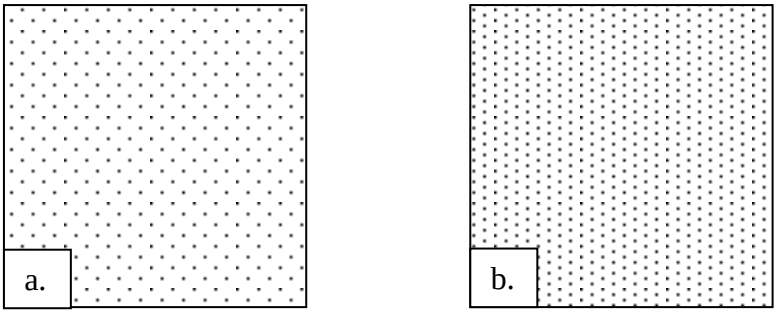

Figure 3.13: Schematic Images of Theoretical Model for Effective Thermal Conductivity Estimation: a. Maxwell-Eucken; b. Effective Medium Theory.

Table 3.2: Comparison the Effective Thermal Conductivity between Theoretical Results and LBM.

$K_1 : K_2$	**Maxwell-Eucken** ($W.m^{-1}.K^{-1}$)	**Effective Medium Theory** ($W.m^{-1}.K^{-1}$)	**Calculated Value** ($W.m^{-1}.K^{-1}$)
1:1	1	1	1
1:2	1.51	1.36	1.50
1:5	2.50	2.16	2.23
1:10	3.33	3.20	2.71
1:20	4.03	4.93	3.05
1:50	4.65	9.38	3.45

3.1.3.2. Comparison with Experimental Data

Furthermore, as verification of the approach, the enhanced LB model was used to evaluate the effective thermal conductivity of two-solid components composite with copper particles dispersed inside the solder matrix [45]. The specific thermo-physical properties of copper and solder are presented in Table 3.3.

Table 3.3: The specific Thermo-physical Properties of Copper and Solder at *300 K.*

Items	**Copper**	**Solder**
Density ($g \cdot cm^{-3}$)	8.94	7.36
Specific heat ($J \cdot g^{-1} \cdot K^{-1}$)	0.384	0.305
Thermal Conductivity ($W \cdot cm^{-1} \cdot k^{-1}$)	3.98	0.781

The effective thermal conductivities for composites with various copper volume fractions were measured and published by H. J. Lee and R. E. Taylor [45]. After comparing the results (Table 3.4), the deviation percentage was computed with the equation:

$$Deviation\ \% = \frac{K_{cal} - K_{exp}}{K_{exp}} * 100 \tag{97}$$

A good agreement is shown in the above table with deviations less than 7%. It is expected that precisely scanned structure profiles would lead to closer agreements. Without knowing the precise composite structure, how the dimension of copper particles influences the effective thermal conductivities could not be presented in the prediction made by the LBM approach.

Table 3.4: Experimental Value and Estimated Value of Effective Thermal Conductivities for the Copper/Solder Composites at *300 K*.

No.	Volume fraction		Thickness (cm)	K_{exp} $(w \cdot cm \cdot K^{-1})$	K_{cal} $(w \cdot cm^{-1} \cdot K^{-1})$	Deviation (%)
	Copper	Solder				
1-1	0.2847	0.7153	0.5089	1.24	1.17	-5.65
1-2	0.1195	0.8805	0.7959	0.955	0.918	-3.87
2-1	0.0124	0.9876	0.4077	0.798	0.792	-0.81
2-2	0.0136	0.9864	0.480	0.800	0.795	-0.66
2-3	0.0286	0.9714	0.3251	0.820	0.805	-1.83
2-4	0.0507	0.9493	0.4858	0.852	0.832	-2.35
2-5	0.0996	0.9004	0.4445	0.924	0.878	-4.98
3-1	0.0195	0.9805	0.4288	0.808	0.803	-0.63
3-2	0.0263	0.9737	0.4961	0.817	0.807	-1.22
3-3	0.0286	0.9714	0.4679	0.820	0.809	-1.34
3-4	0.1029	0.8971	0.4679	0.927	0.882	-4.84
3-5	0.2377	0.7623	0.6038	1.154	1.073	-7.02
4-1	0.0848	0.9152	0.5156	0.902	0.866	-3.99
4-2	0.1586	0.8414	0.4536	1.02	0.949	-6.96
4-3	0.2516	0.7484	0.474	1.18	1.135	-3.81
4-4	0.2894	0.7106	0.5027	1.25	1.172	-6.24
4-5	0.2910	0.709	0.5184	1.25	1.178	-5.76

The estimated effective thermal conductivities are always smaller than the measured data. This is mainly due to the fact that the model is designed at ambient temperature and has neglected the effects of thermal convection and radiation. The radiative component could play a role for metal composites at high temperature level. Secondly, the fiber volume fraction applied in the model is only an approximation close to the real value due to the programming limits, resulting in smaller conductivities. Finally, the obtained data from experiments and calculation were plotted in Figure 3.16 for comparison.

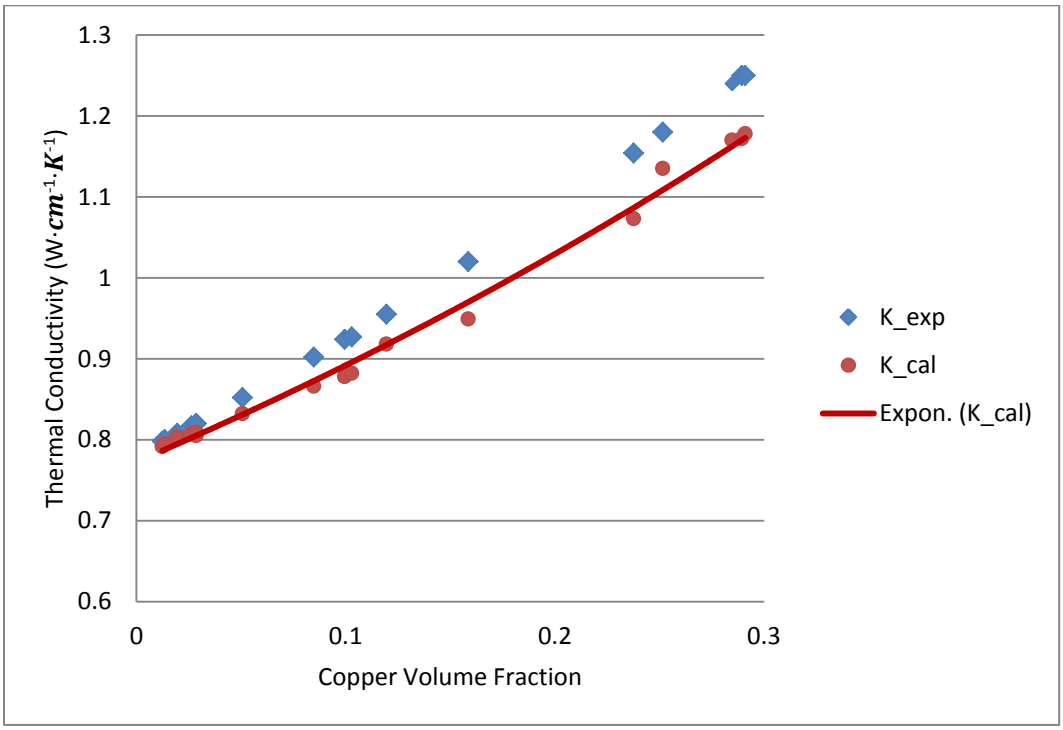

Figure 3.14: Comparison of the Experimental K_{eff} and the Estimated K_{cal} Effective Thermal Conductivities for the Copper/Solder Composites (Fitted in an Exponential Trend).

3.2. Discussion of Thermal Properties of Porous Media

3.2.1. Temperature Distribution and Temperature Evolution

Upon verifying the accuracy of the LBM model, the temperature profile for a porous media described in Figure 3.14 is simulated as shown in Figure 3.17. The temperature profile within the structure is presented in Figure 3.18 from the transient state to the steady state.

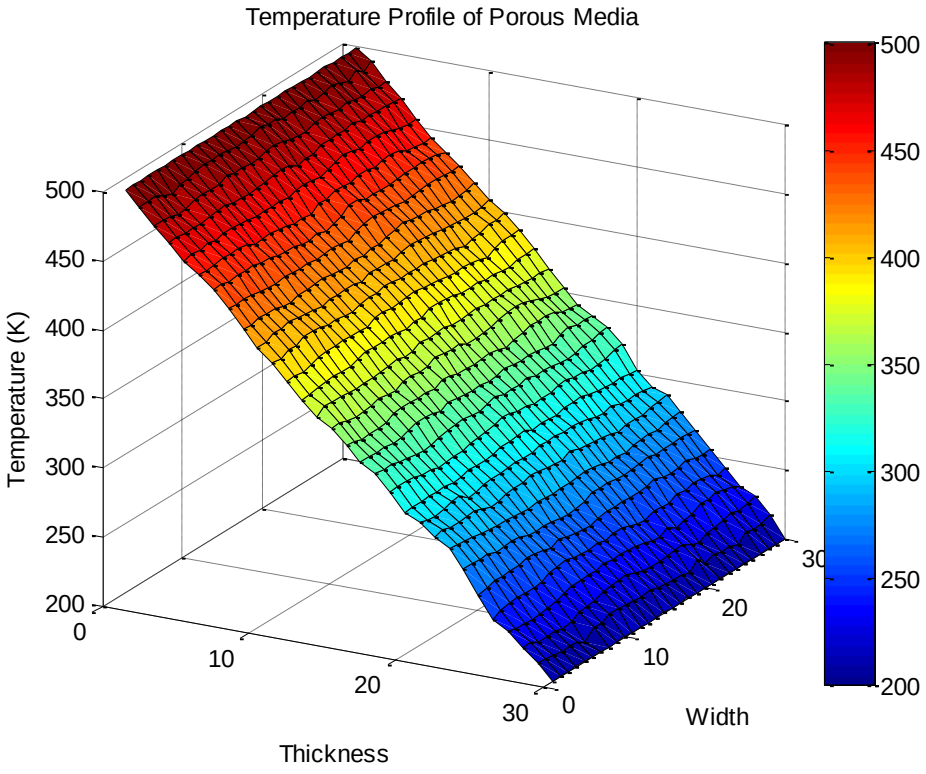

Figure 3.15: Temperature Profile Simulated in 3D for a Randomly Generated Porous Media.

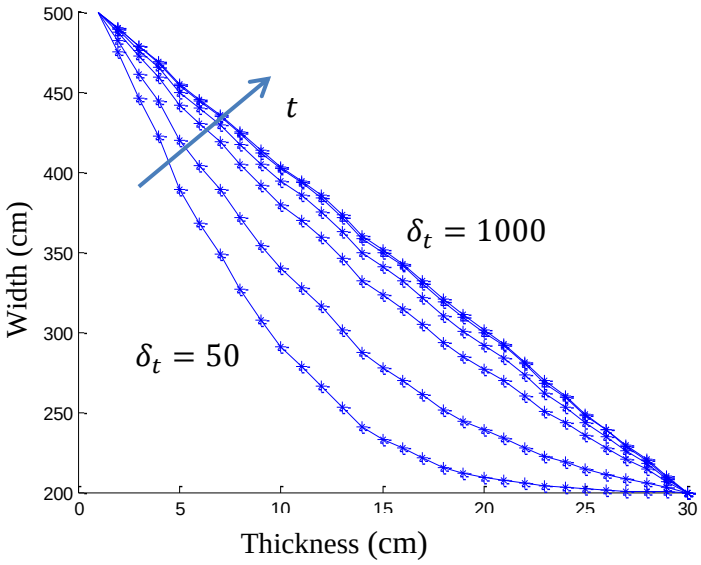

Figure 3.16: Temperature Evolution at x=thickness/2 at Time Steps:

$\delta_t = 50, 100, 200, 300, 500, 1000.$

3.2.2. Prediction of the Relationship between Fiber Volume Fraction and the Effective Conductivity

In order to find out the relationship between the fiber volume fraction and the effective thermal conductivities of two-component composites, nine fiber volume fractions are considered from 10% to 90%, so that the model can be validated for a wide range of applications:

$$f_v = 10\%, 20\%, 30\%, 40\%, 50\%, 60\%, 70\%, 80\%, 90\% \quad (98)$$

As previously explained, since the model can only generate structures with approximate fiber volume fractions of specified values, thus, five data points for each percentage are randomly adapted for higher accuracy. Additionally, although structures have same fiber volume fraction, the fiber orientation distribution and porosity are different from one another.

Therefore, it is necessary to have enough data points for an average value to represent such a structural variation. The effective thermal conductivities are estimated with the LB model for each replicate and shown in Table 3.5.

Finally, the total 35 data points were plotted in Figure 3.19 and analyzed by setting up a second-order polynomial regression model in a statistical software package, R. The Figure indicates that the effective thermal conductivity increases with the fiber fraction in a non-linear basis, which is consistent with the results published in the literature [30]. This is explained by the fact that the volume of trapped air is reduced while the amount of fiber by unit volume is increasing, then thermal resistance mainly provided by the gas phase declines. By examining the output from R, P-value for the second order polynomial term is significantly small ($p - value = 2 * 10^{-16}$). Therefore, a statistical conclusion can be made illustrating the same trend that the effective thermal conductivities are not linearly associated with the volume fraction of solid phase.

The results estimated by the Maxwell-Eucken and the Effective Medium Theory models were plotted together with the results predicted with the LBM model as a comparison. A similar relationship between the fiber fraction and the thermal conductivities were obtained, though differences on values existed because of the structure issues previously explained. The figure also showed that the thermal conductivities calculated from the LBM model is in between of the values from series mode and the parallel mode.

Table 3.5: Effective Thermal Conductivities ($W.m^{-1}.K^{-1}$) Estimated for the Porous Structures with Different Fiber Fractions.

$\emptyset_f$	k_{eff}	$\emptyset_f$	k_{eff}	$\emptyset_f$	k_{eff}	$\emptyset_f$	k_{eff}	$\emptyset_f$	k_{eff}
0.90	1.96	0.91	1.97	0.90	1.91	0.91	1.97	0.90	1.94
0.80	1.55	0.80	1.54	0.81	1.56	0.81	1.58	0.76	1.46
0.71	1.33	0.72	1.32	0.70	1.31	0.68	1.24	0.70	1.30
0.59	1.07	0.59	1.06	0.61	1.09	0.59	1.08	0.61	1.10
0.52	0.96	0.49	0.93	0.49	0.94	0.49	0.93	0.50	0.94
0.38	0.78	0.41	0.80	0.38	0.80	0.41	0.83	0.39	0.80
0.30	0.72	0.29	0.70	0.27	0.68	0.33	0.74	0.31	0.73
0.20	0.63	0.21	0.63	0.22	0.64	0.20	0.63	0.18	0.62
0.10	0.56	0.11	0.56	0.08	0.54	0.12	0.57	0.09	0.55

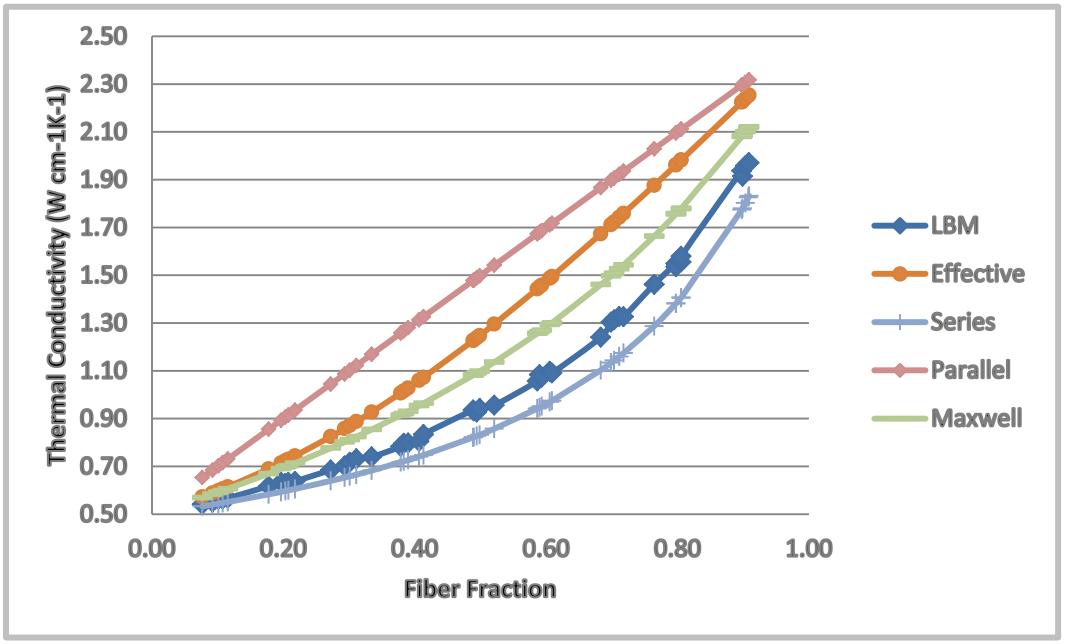

Figure 3.17: Effective thermal conductivity VS. volume fraction of fibers in different modes.

4. Conclusion:

A Lattice Boltzmann model was proposed, adapted and applied to simulate heat transfer through bi-component composites. After applying isothermal and insulated conditions for the boundaries, the model was validated by comparing with simple two dimensional configurations, theoretical approximations and some published experimental data. Good agreements were obtained. Therefore, the model can be applied to predict and assess the trend of effective thermal conductivity of composites with the increase of fiber volume fraction. The present model is not only applicable for porous media, such as nonwovens, but also suitable for most if not all bi-component composites. Additionally, since no empirical parameters have to be determined case by case, the model is quite useful to simulate the thermal conduction in materials with complex porous structures.

5. Future Work

5.1. Three-dimensional Lattice Boltzmann model

For a more realistic simulation of the effective thermal conductivity in porous media, using a three-dimensional Lattice Boltzmann model will provide results more accurate than the D2Q9 model applied in this study. A conventional and successful 3D model is proposed as D3Q15, where the motion of interacting particles in the third direction is considered. Therefore, there are 15 discrete velocities, e_α, applied, so that the streaming and collision notions of particles can be represented three-dimensionally. [46, 47]

$$\boldsymbol{e_\alpha} = \begin{cases} (0,0,0) & \alpha = 15 \\ (\pm 1,0,0)c, (0,\pm 1,0)c, (0,0,\pm 1) & \alpha = 1\ to\ 6 \\ (\pm 1,\pm 1,\pm 1)c & \alpha = 7\ to\ 14 \end{cases} \tag{99}$$

The evolution equation introduced in the Lattice Boltzmann method is still valid for the D3Q15 model; whereas the equilibrium distribution, g_α^{eq}, is modified as:

$$g_\alpha^{eq} = \begin{cases} 0 & \alpha = 15 \\ \frac{1}{9}T & \alpha = 1\ to\ 6 \\ \frac{1}{24}T & \alpha = 7\ to\ 14 \end{cases} \tag{100}$$

Then the equilibrium distribution can be calculated with the local temperature T.

The dimensionless relaxation time for each component is determined by the individual thermal conductivity, K_n, and specific heat, ρC_p.

$$\tau = \frac{9}{5}\frac{K_n}{(\rho C_p)c^2\delta_t} + 0.5 \tag{101}$$

The interface continuity and the boundary treatments in the D2Q9 model are still applicable for this three-dimensional model. Then the macroscopic temperature and heat flux can be calculated with equation (50) and (51), where the 9 velocities are replaced with the 14 velocities. The effective thermal conductivity is solved with the steady heat flux through the system cross-section area, dA, between the temperature gradient, ΔT, with a distance, L, as shown in the Equation (52).

Although the two-dimensional Lattice Boltzmann model has shown a great agreement with realistic results, the three-dimensional model has been provided a better agreement, especially dealing with the measurements based on transient comparative methods [46].

5.2. Association with Micro-Structural Images

One of the outstanding advantages for Lattice Boltzmann method is the ease of simulating the properties of those materials with multi-component/phase and complex geometries. Without knowing the fine structure, the predicted results might have considerable error. Thus, the model would provide more promising estimations when associating with images of micro-structures.

The images can be obtained with a microscope (Figure 5.1.a), for example Scanning Electron Microscope Technique, or random generation-growth algorithm (Figure 5.1.b) which is introduced by Moran Wang in their studies [30]. The fibrous structure is generated based on a core distribution, fiber orientation angle, fiber length and diameter.

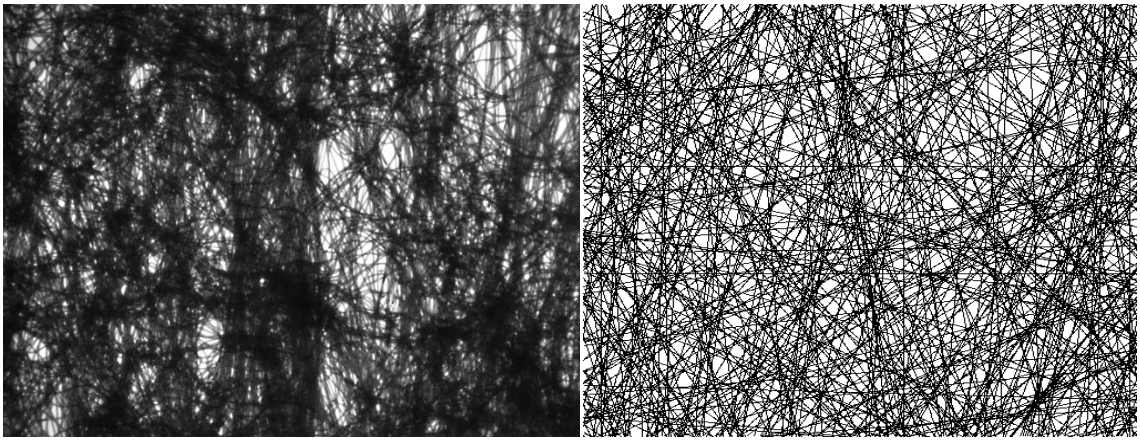

Figure 5.1: Images with Micro-structures of Nonwoven Materials: a. Image Captured by Microscope; b. Image Generated with the Fiber Orientation Distribution.

Once the images are obtained independently of the method, they are discretized into grids, so that the micro particles could be statistically encapsulated on lattices, where the fiber phase is defined as 1 and the gas phase as 0 in the binary meshes. According to the images, the lattice unit, δ_x, is determined. Therefore, the real condition can be simulated precisely [30].

5.3. Experimental Assessment of Needle-punched Nonwovens

The micro-structure of nonwovens and fibrous assemblies play a significant role on determining their thermal and mechanical properties. The structure is closely dependent on the web forming and bonding technologies applied. Moreover, different production configurations would provide a large structural variation for each process. Large amount of fibrous thermal insulators are produced with needle-punching process for a bulky structure. Therefore, after obtaining the thermal properties with the fine scanning images of needle-punched fabrics, it is also interesting to learn how production configurations impact the micro-structures and further the thermal performances.

The configurations that are of interest include the types of needles selected for processing, the penetration depth, needling density and the number of needling passes. A primary experimental design is shown in Table 5.1: a bulky PET or fiberglass insulator is produced with two different needle type combinations. After the fabrics are manufactured with the specified configurations, the thermal conductivity will be measured with the Guarded-Hot-Plate Apparatus and compared with the predicted values from the model.

Proper needle types are selected closely according to the fiber type, fiber fineness and the property requirements of the final products. Not only the needle gauge, but also barb shape and barb size are all essential factors that need to be considered carefully. Each of them would significantly influence the final structure of the fabric. The number of working barbs is determined by controlling the penetration depth, which is generally defined as the distance between the needle tip and the upper surface of the bed plate. About 85% fiber transfer is done by the first three barbs, thus, it is of importance to balance the efficiency with needle

breakage and hand feel of final products. Deeper the needles penetration through the fabric, the more fibers are transferred resulting in dense structures and more needle breakages.

Table 5.1: Experimental Design for Assessing the Thermal Conductivities of Needle-Punched Fabrics.

C/S	Polymers	Basis Weight (gsm)	Needle type	Passes	No.	Punch density	Penetr. Depth (cm)	k_{exp}	k_{cal}
Staple	fiberglass	400	Type 1	1	1	Low	Low		
					2	High	Low		
					3	Low	High		
					4	High	High		
				2	5	Low	Low		
					6	High	Low		
					7	Low	High		
					8	High	High		
			Type 2	1	9	Low	Low		
					10	High	Low		
					11	Low	High		
					12	High	High		
					13	Low	Low		
					14	High	Low		
					15	Low	High		
					16	High	High		

Needling density, also called density of punch, is the number of punches per area (punch/m^2) [49, 50].

$$N_p = \frac{D_n * f_n * Np}{v_n} \tag{102}$$

Where:

D_n: *Needle density, total number of needles per 1 meter of working width*

f_n: *Frequency of needle punching (s^{-1})*

Np: *Number of passes through needle loom (or number of needle looms)*

v_n: *Velocity of web (ms^{-1})*

A statistical model could be set up with the programming software, SAS, having the configurations as the predictors and the thermal conductivity as the response. The association can be assessed by fitting a multiple-factor ANOVA. The main effects of each parameter can then be inferred, and the interaction of one another could be also considered in the model.

6. REFERENCES

1. Trevor J. Cox and Peter D'antonio, Acoustic Absorbers and Diffusers, (Taylor & Francis, New York, NY, 2004), pp. 129.
2. Yilmaz, Nazire Deniz. Acoustic properties of Biodegradable Nonwovens, pp12-14
3. Tamotsu Kawasaki, Yokohama, Evacuated Heat Insulation Unit, United States Patent: Patent Number: 4, 669, 632, 1985.
4. Worldometers: World Statistics Updated in Real Time http://www.worldometers.info/cars/.
5. Val Yachmenev, Loan Negulescu And Chen Yan, Thermal Insulation Properties of Cellulosic-based Nonwoven Composites, Journal of Industrial Textiles, 2006 pp 36-73.
6. news.bbc.co.uk/2/hi/science/nature/7262747.stm.
7. Nehdi M, Khan A. Cementitious composites containing recycled tire rubber: an overview of engineering properties and potential applications. Cement Concrete and Aggregates 2001; 23:3–10.
8. Siddique R, Naik TR. Properties of Concrete Containing Scrap-Tire Rubber – An Overview. Waste Manage 2004; 24:563–9.
9. Bulent Yesilata, Yusuf isiker and Paki Turgut, Thermal Insulation Enhancement in Concretes by Adding Waste PET and Rubber Pieces, Construction and Building Materials 23(2009) 1878-1882.
10. Craig M. Clemons and Daniel F. Caulfield, Natural fiber, (196-206), 2005.

11. Maya Jacob John, Sabu Thomas, Biofibers and biocomposites, Carbohydrate Polymers 71 (2008) 343-364.
12. Rajesh D. Anandjiwala, Sunshine Blouw, Composites from Bast Fibres Prospects and Potential in the Changing Market Environment, Journal of Natural Fibers, Vol. 4(2) 2007.
13. Paul Wambua, Jan Ivens, Ignaas Verpoest, Natural fibers: can they replace glass in fiber reinforced plastics? Composites Science and Technology 63 (2003) 1259–1264.
14. A.K. Mohanty, M.Misra and G.Hinrichsen, Biofibers, Biodegradable Polymers and Biocomposites: An Overview, Marcromolecular Materials and Engineering, 276/277, 1-24 (2000).
15. V. G. Yachmenev, D. V. Parikh and T. A. Calamari, Thermal Insulation Properties of Biodegradable, Cellulosi-Based Nonwoven Composites for Automotive Application, Journal of Industrial Textiles 2002; 31;283.
16. Benjamin Gebhart, Heat Conduction And Mass Diffusion, 1993, page 440-442.
17. J. Fricke, D. Biittner, R. Caps, J. Gross and O. Nilsson, Solid Conductivity of Loaded Fibrous Insulations, Insulation Materials, Testing, and Application, 1990 pp66-78.
18. Robert Siegel and John R. Howell, Thermal Radiation Heat Transfer, Third Edition, 1992, 522-524.
19. Anastasios Karamanos, Agis Papadopoulos and Dimitrios Anastasellos, Heat Transfer Phenomena in Fibrous Insulating Materials, 2004, Geolan.gr http://www.fibran.gr/sappek/docs/publications/article_6.pdf.

20. Markus Spinnler, Edgar R.F. Winter, Raymond Viskanta, Thomas Sattelmayer, Theoretical Studies of High-temperature Multilayer Thermal Insulations Using Radiation Scaling, Journal of Quantitative Spectroscopy & Radiative Transfer 84 (2004) 477-491.
21. Kamran Daryabeigi, Stephen D.Miller and George R.Cunnington, Heat Transfer in Hihg-Temperature Multilayer Insulation.
22. Kamran Daryabeigi, Heat Transfer in High-Temperature Fibrous Insulation, 8th AIAA/ASME Joint Thermophysics and Heat Transfer Conference, 24-26 June 2002.
23. Benoit Cushmann-Roisin, Building Energy Needs with Particular Attentions Paid to Thermal Insulation, Jan, 2011.
24. Bulent Yesilata, Paki Turgut, a Simple Dynamic Measurement Technique for Comparing Thermal Insulation Performance of Anisotropic Building Materials, Energy and Building 39 (2007) 1027-1034.
25. Sujan P. Kulkarni & C.Vipulanandan, Thermal Conductivity of Insulators, http://www2.egr.uh.edu/~civeb1/CIGMAT/03_poster/10.pdf.
26. ASTM C177-97 Standard Test Method for Steady-State Heat Flux Measurements and Thermal Transmission Properties by Means of the Guarded-Hot-Plate Apparatus.
27. Thermal Conductivity: http://www.hitemp707.com/ASTMThermalConductivity.pdf.
28. Michael C.Sukop, Daniel T.Thorne,Jr., Lattice Boltzmann Modeling-An Introduction for Geoscientists and Engineers, 2006.
29. Jian Guo Zhou, Lattice Boltzmann Methods for Shallow Water Flows, 2004.

30. Moran Wang, Jihuan He, Jianyong Yu, Ning Pan, Lattice Boltzmann Modeling of the Effective thermal Conductivity for Fibrous Materials, International Journal of Thermal Sciences 46 (2007) 848-855.
31. Xiaoyi He, Shiyi Chen and Gary D.Doolen, A Novel Thermal Model for the Lattice Boltzmann Method in Incompressible Limit, Journal of Computational Physics 146, 282-300 (1998).
32. Annunziata D' Orazio, Massimo Corcione, Gian Piero Celata, Application to Natural Convection Enclosed Flows of a Lattice Boltzmann BGK Model Coupled with a General Purpose Thermal Boundary Condition, International Journal of Thermal Sciences 43 (2004) 575-586.
33. Y. Peng, C. Shu, and Y. T. Chew, Simplified Thermal Lattice Boltzmann Model for Incompressible Thermal Flows, Physical Review E 68, 026701 (2003) .
34. Raoudha Chaabane, Faouzi Askri, Sassi Ben Nasrallah, Application of the Lattice Boltzmann Method for Solving Conduction Problems With Heat Flux Boundary Condition, International Renewable Energy Congress, November 5-7, 2009-Sousse Tunisia.
35. Xi Chen, Peng Han, A Note on the Solution of Conjugate Heat Transfer Problems Using SIMPLE-like Algorithms, International Journal of Heat and Fluid Flow 21 (2000) 463-467.
36. Qun Chen, Moran Wang, Ning Pan, Zeng-yuan Guo, Irreversibility of Heat Conduction in Complex multiphase Systems and Its Application to the Effective

Thermal Conductivity of Porous Media, International Journal of Nonlinear Sciences and numerical Simulation, 10(1), 7-16, 2009.

37. Zou, Q.S. and He X.Y., On Pressure and Velocity Boundary Conditions for the Lattice Boltzmann BGK Model, Physics of Fluids, 1997. 9 (6), 1591-1598.
38. Boundary Conditions: http://www.lbmethod.org/models:bc.
39. M.R.Arab, B.Pateyron, M. EI Ganaoui and N. Calve, Lattice Boltzmann Simulations for Thermal Conductivity Estimation in Heterogeneous Materials, Defect and Diffusion Forum Vols. 283-286 (2009) pp364-369.
40. K.S. Reddy and Karthikeyan P, Combinatory Models for Predicting the Effective Thermal Conductivity of Frozen and Unfrozen Food Materials, Advances in Mechanical Engineering, Volume 2010, pp14.
41. B.M. Caruta, New Developments in Materials Science Research, 2007, pp100-104.
42. M. M. Awad, Y.S. Muzychka, Effective Property Models, for Homogeneous Two-Phase Flows, Experimental Thermal and Fluid Science 33 (2008), pp106-113.
43. A. Padilla, A. Sanchez-Solis and O. Manero, A Note on the Thermal Conductivity of Filled polymers, Journal of Composite Materials 1988 22:616.
44. Moran Wang, Jinku Wang, Ning Pan and Shiyi Chen, Mesoscopic Predictions of the Effective Thermal Conductivity for Microscale Random Porous Media, Physical Review E 75, 036702 (2007).
45. H.J.Lee and R.E.Taylor, Thermal Diffusivity of Dispersed Composites, Journal of Applied Physics, Vol.47, No.1, Jan.1976.

46. Moran Wang, Jinku Wang, Ning Pan, Shiyi Chen and Jihuan He, Three-dimensional Effect on the Effective Thermal Conductivity of Porous Media, J.Phys.D: Appl. Phys. 40 (2007) 260-265.

47. Moran Wang, Qinjun Kang, Ning Pan, Thermal Conductivity Enhancement of Carbon Fiber Composites, Applied Thermal Engineering 29 (2009) 418-421.

48. Junku Wang, Moran Wang and Zhixin Li, A Lattice Boltzmann Algorithm for Fluid-Solid Conjugate Heat Transfer, International Journal of Thermal Sciences 46 (2007) 228-234.

49. R. Senthil Kumar, http://www.scribd.com/doc/3196988/5-Needlepunching.

50. A T Purdy MSC PhD CText ATI, Needle-punching, The Textile Institute 1980.